CALCULATION OF A CONSTITUTIVE POTENTIAL FOR ISOSTATIC POWDER COMPACTION

*S. J. Subramanian and P. Sofronis**

University of Illinois at Urbana-Champaign
Department of Theoretical and Applied Mechanics
216 Talbot Laboratory
104 S. Wright Street, Urbana IL 61801

June 2001

* To whom all correspondence should be addressed, email: sofronis@uiuc.edu; fax: (217) 244 5707

ABSTRACT

A macroscopic constitutive potential has been developed for the deformation of a powder compact of cylindrical particles during pressure sintering. The derivation is based on finite element simulations of the densification process that proceeds under the synergistic action of power-law creep deformation in the particles, evolution of the nonlinearly developing contact area between the particles, and interparticle and pore free-surface diffusional mass transport. Solution to this initial-boundary value problem provides all necessary information for the calculation of the constitutive potential. The associated constitutive law predicts the densification rate of the powder compact at a given temperature and pressure in terms of material parameters such as creep constants and diffusion coefficients, and reflects the role played in the densification process by various micromechanical features such as the pore surface curvature. The model predictions are compared with existing analytical models for plane strain densification and experimental data from sintering of copper wires by stress-driven grain boundary and curvature-driven pore surface diffusion.

Keywords: sintering, constitutive law, diffusion, creep deformation.

1. INTRODUCTION

It is well known that in powder densification the closing of porosity occurs by the synergistic action of various deformation mechanisms such as linear elasticity, rate-independent plasticity, power-law creep, diffusion along the interparticle contacts and pore surfaces, and interparticle slip (Ashby, 1974; Swinkels and Ashby, 1981; Helle *et al.*, 1985). Description of the macroscopic strain response of a powder compact (McMeeking, 1992) under load in terms of constitutive potentials that account for the deformation mechanisms at the microscale at a given temperature offers an efficient means to simulate and analyze real-world component densification through user material routines in general purpose finite element codes (Abouaf *et al.*, 1988; Govindarajan and Aravas 1994a, b; Kim *et al.*, 1998). The method of devising constitutive potentials to predict the overall densification response of a powder under given stress and temperature was first employed by Kuhn and McMeeking (1992) in evaluating the stage I response of a powder compact that densifies under power-law creep deformation in the bulk of the particles. McMeeking and Kuhn (1992) proposed a corresponding potential for a densifying powder when the controlling densification mechanism is interparticle diffusion. A macroscopic yield surface for a random aggregate of rigid, perfectly plastic spheres was developed by Fleck *et al.* (1992) in which it was assumed that plastic deformation occurs in the region adjacent to the contacts between the particles. Akisanya and Cocks (1994) and Akisanya et al. (1995) studied the deformation of rigid, perfectly plastic cylinders under both hydrostatic and non-hydrostatic loading situations, and derived constitutive models using slip line field and finite-element methods. Fleck (1995) examined the effect of interparticle friction and anisotropy in the distribution of the contact areas, the number of contacts per unit surface area of particles, and hardness of each contact on the macroscopic yield locus. Alternatively, a crystal plasticity approach was taken by Fleck (1995) to devise the yield surface for the cold compaction of an aggregate in which the contacts were treated as compaction planes capable of yielding under shear and normal straining and thus the particles were modeled as single crystals with a set of slip planes along the assumed compaction planes. Most recently, Storakers *et al.* (1999) have developed constitutive equations for the early stages of cold and hot compaction occurring by viscoplastic deformation of initially randomly packed powders.

The theoretical framework for developing constitutive potentials for the densification of powder compacts under the synergistic action of the densification mechanisms has been laid out in the work of Cocks (1994). Essentially, by using the principle of virtual power to equate external and internal dissipation, and by averaging the results over representative volume elements, one can predict

the macroscopic behavior of a powder in response to an applied stress, and in turn the densification rate at given load and temperature conditions (McMeeking, 1992). Thus, Cocks (1994) and Cocks and Aparicio (1995) by using appropriate admissible stress or velocity fields calculated bounds on the form of the macroscopic potentials that govern the constitutive behavior of a powder under the action of specific densifying mechanisms. Significantly, in these calculations, Cocks (1994) considered the interaction between pairs of concurrently acting mechanisms in effecting the overall compaction of the aggregate. It should be mentioned that constitutive potentials for the deformation of plastically deforming rate independent solids (Gurson, 1977; Guennouni and Francois, 1988: Leblond *et al.*, 1995) or power-law creeping solids (Duva and Hutchinson, 1984; Duva, 1986; Guennouni and Francois, 1987; Ponte Castaneda and Willis, 1988; Cocks, 1989; Sofronis and McMeeking, 1992; Leblond *et al.*, 1994; Kailasam and Ponte Castaneda, 1996) have also been used to describe the response of porous materials respectively in the context of room temperature ductile fracture or high temperature creep failure. More specifically, rigorous homogenization theories for the macroscopic response of voided materials with evolving microstructure have been given recently by Ponte Castaneda and Zaidman (1994), Ponte Castaneda (1997), Ponte Castaneda and Suquet (1998), and Kailasam *et al.* (2000).

In the present work, a constitutive potential for the deformation of an aggregate of long cylindrical particles is to be devised when densification takes place under the concurrent action of power-law creep in the bulk of the particles along with interparticle and pore free-surface diffusion. Densification is simulated to begin with the initial contact between particles established by instantaneous power-law creep deformation, and proceeds in time through combined power-law creep deformation in the bulk coupled with diffusional mass transport on the interparticle contact areas and pore surfaces. Additional important ingredients in the present model are the enforcement of the classical Laplace relationship between the curvature, energy of the pore surface, and the normal stresses in the adjoining bulk material (Herring, 1951; Rice and Chuang, 1981; Freund *et al.*, 1993), and the monitoring of the evolution of the interparticle contact area as deformation proceeds. Solution to the relevant initial-boundary value problem (Subramanian and Sofronis, 2001) at a given applied macroscopic stress provides information on the values of both microscopic (e.g. flux, free surface curvature) and macroscopic parameters (e.g. strain rate) needed to construct the constitutive potential for the compact by following the methodology of Sofronis and McMeeking (1992) and Cocks (1994).

In the numerical calculations, densification of a square array of cylinders under hydrostatic loading is considered in order to simulate hot isostatic pressing (HIPing). Pure HIPing was considered solely to reduce the degree of numerical complexity that would arise respectively from interparticle slip if the applied macroscopic stress had a nonzero deviatoric component. Similarly the creep deformation within the particles was modeled in the small displacement regime to avoid the complexities of large strain formulation in the coupling of the contact area evolution with the densification mechanisms. Thus, the numerical results pertain only to small density changes from the initial undeformed stage of the compact. A finite element formulation with no nodal updating was employed in a unit cell to solve the relevant initial boundary value problem under plane strain conditions (Subramanian and Sofronis, 2001). It should be mentioned that the present calculation of the constitutive potential by the finite element method is equally valid for general loading states, though an appropriate unit cell has to be chosen to solve the relevant densification problem and suitable modifications to the governing equations have to be made to account for interparticle slip (Needleman and Rice, 1980).

2. MATERIAL CONSTITUTIVE LAWS

The bulk of the particles is incompressible and obeys the creep law

$$\dot{\varepsilon}_{ij} = \frac{\partial \phi^c}{\partial \sigma_{ij}}, \tag{1}$$

where $\dot{\varepsilon}_{ij} = \left(v_{i,j} + v_{j,i}\right)/2$ is the creep strain rate, v_i is the velocity, ϕ^c is the creep potential such that

$$\phi^c = \frac{1}{1+n}\dot{\varepsilon}_0 \sigma_0 \left(\frac{\sigma_e}{\sigma_0}\right)^{1+n}, \tag{2}$$

$\sigma_e = \sqrt{3 s_{ij} s_{ij}/2}$ is the effective stress, $s_{ij} = \sigma_{ij} - (\sigma_{kk}/3)\delta_{ij}$ is the deviatoric stress, n is the creep exponent, $\dot{\varepsilon}_0$ and σ_0 are material parameters in the uniaxial tension relation $\dot{\varepsilon}/\dot{\varepsilon}_0 = \left(\sigma/\sigma_0\right)^n$, δ_{ij} is the Kronecker delta, $(.)_{,j} = \partial(.)/\partial x_j$, and the superposed dot denotes differentiation with respect to time. From Eqs. (1) and (2), one finds that $\dot{\varepsilon}_{ij} = 3C\sigma_e^{n-1} s_{ij}/2$, where $C = \dot{\varepsilon}_0/\sigma_0^n$ is the creep modulus.

Diffusion along the interparticle contact areas or the pore surface is driven by chemical potential gradients (Herring, 1951; Chuang *et al.*, 1979) such that

$$j_b = \mathcal{D}_b \, d\sigma_n/ds \tag{3}$$

along the interparticle area, and

$$j_p = \mathcal{D}_p \, d(\gamma_p k)/ds \tag{4}$$

along the pore surface. Here, j_b and j_p are the volumetric fluxes per unit length along a direction s tangential to the interparticle and the pore surface areas respectively (see Figs. 1a and 1b), $\mathcal{D}_b = D_b \delta_b \Omega / KT$ and $\mathcal{D}_p = D_p \delta_p \Omega / KT$ are correspondingly interparticle and pore surface diffusivities having dimensions of volume divided by stress per unit time, D_b and D_p are the corresponding diffusion coefficients, δ_b and δ_p are the corresponding effective thicknesses through which matter diffuses, σ_n is the stress normal to the contact area between the particles, k and γ_p are respectively the curvature and the energy of the pore surface (Figs. 1a and 1b), Ω is the atomic volume of the diffusing species, K is Boltzmann's constant, and T is the absolute temperature. Further, the tangential stresses vanish everywhere on the interparticle contact areas since these are assumed to be freely slipping.

In order to describe matter conservation on the interparticle contacts (Subramanian and Sofronis, 2001), let $\dot{h}(s)$ be the normal overlapping rate that would have resulted had the particles been free to penetrate into one another under the action of external load. Since the particles in reality do not plough into each other, all the mass that would otherwise interpenetrate is assumed to be transported along the contact areas by interparticle diffusion. Then, matter conservation along the interparticle contact area requires

$$\frac{dj_b(s)}{ds} + \dot{h}(s) = 0. \tag{5}$$

For the calculation of $\dot{h}(s)$, consider two points on the boundaries of particles I and II with corresponding velocities v_i^I and v_i^{II} (see Fig. 1a). Note that v_i^I and v_i^{II} are the velocities of points on the particle surfaces on each side of the interface that develops when the particles come into contact. Since the points are initially a distance $\Delta g(s)$ apart (Fig. 1a), the normal overlapping rate $\dot{h}(s)$ is expressed as

$$\dot{h}(s) = \left(v_i^I(s) - v_i^{II}(s)\right) n_i + \dot{g}(s) = v_n(s) + \dot{g}(s), \tag{6}$$

where $v_n(s)$ is the relative normal velocity of approach, n_i are the components of the unit normal to the contact area (see Fig. 1a), and $\dot{g}$ is the rate of change of the gap Δg. In other words, the entire relative normal velocity does not contribute to the mass flux when these two points come into contact; part of it goes toward bridging the gap. Of course, for points that are already in contact, $\Delta g = 0,\ \dot{g} = 0,\ \dot{h}(s) = v_n(s)$, and thus the entire relative normal velocity v_n results in a change of the volumetric flux. In this case, one recovers the form of the matter conservation equation employed by Needleman and Rice (1980) in their study of diffusive cavitation along grain boundaries.

Along the pore surface, matter conservation dictates that

$$\frac{dj_p}{ds} + \dot{\alpha}(s) = 0\,, \tag{7}$$

where $\dot{\alpha}(s)$ is the local particle expansion rate (Fig. 2), measured normal to the particle surface, and is positive when matter is deposited on the pore surface and negative when the pore surface is eroded. Here it should be emphasized that though the rate $\dot{\alpha}$ relates to the flux on the pore surface just as the normal relative velocity v_n does to the flux on the interparticle contact areas, $\dot{\alpha}$ is not the velocity of any material point on the pore surface; it is simply the rate at which mass is added to or removed from the pore surface.

Equilibrium at any arbitrary point on the pore surface is described by the standard Laplace equation (Gurtin and Murdoch, 1975; Rice and Chuang, 1981; Freund *et al.*, 1993) that relates the normal stress σ_n from the adjoining bulk material to the local curvature k

$$\sigma_n(s) = \gamma_p\, k(s). \tag{8}$$

In the present model, surface tension γ_p is assumed to be constant and therefore, the tangential stress on the pore surface is zero (Rice and Chuang, 1981; Freund *et al.*, 1993). The sign conventions for curvature and normal stress are shown in Fig. 1b. At the junction between the interparticle contact area and the pore surfaces (tip), both volumetric flux and chemical potential are continuous. Chemical potential continuity requires that

$$\sigma_0 = \gamma_p\, k_0, \tag{9}$$

where the subscript 0 is used to denote values of σ_n and k at the junction (Fig. 1b).

3. THE UNIT CELL MODEL

The problem of densification of a periodic square array of cylinders under hydrostatic loading in plane strain deformation conditions is considered, and hence the term 'particle' in the remainder of the paper refers to infinitely long cylinders. Due to the symmetry of the square particle arrangement, the densification is studied by considering the deformation of just one quadrant of the cylinder as shown in Fig. 2. This particular choice of unit cell has been made in view of the fact that the normals to the contact areas are known *a priori*. This offers a significant simplification with respect to the numerical evaluation of the contact areas and reduces the number of iterations and computation time considerably. The study of the densification process is carried out by solving the following two coupled problems concurrently (Subramanian and Sofronis, 2001): i) the bulk *deformation of the particle* that also involves the interparticle contact area evolution along with interparticle diffusion, and the effect of the pore surface stress induced by the curvature; and ii) the *pore surface diffusion* for the calculation of the particle expansion $\alpha(s)$ along the pore surface (Fig. 2).

(i) *Deformation of the particle*: Extending the formulation of Needleman and Rice (1980) to include the effects of stress induced by pore surface curvature, one can state the principle of virtual power for the deformation of the particle (Fig. 2) in the following form

$$\int_{S_T} T_i \delta v_i ds = \int_A \sigma_{ij} \delta \dot{\varepsilon}_{ij} dA + \int_{S_b} \sigma_n \delta \dot{h} ds + \int_{S_p} \sigma_n \delta v_n ds$$
$$+\gamma_b \, \delta \dot{a}_1 - \gamma_p \, (\delta v_{tip} \cos\phi)_C + \gamma_b \, \delta \dot{a}_2 - \gamma_p \, (\delta v_{tip} \cos\phi)_D \, . \qquad (10)$$

Here T_i is specified traction on the external boundary S_T of the unit cell, σ_{ij} are the stress components within the bulk region A occupied by the particle, δv_i is an arbitrary virtual variation of the velocity on S_T and in A, $\delta \dot{\varepsilon}_{ij}$ is the corresponding strain rate variation, σ_n is the normal stress either on the interparticle area $S_b = S_{b1} \cup S_{b2}$ or the pore surface area S_p (that is the boundary $S - S_T - S_b$ of the particle deforming by creep before the deposition of the mass transported by surface diffusion, (Fig. 2)), δv_n is the virtual variation of the normal velocity of points on the pore surface S_p, $\delta \dot{h}$ is the virtual rate of $\dot{h}$ along contact area $S_b = S_{b1} \cup S_{b2}$ such that $\delta \dot{h} = \delta v_n + \delta \dot{g} = \delta v_n$ (see Eqn. (6)) since the gap $\Delta g(s)$ is a fixed part of the particle geometry at any instant of time, and ϕ_C and ϕ_D are the dihedral angles at (tip) points C and D and are shown schematically as angle ϕ in Fig. 1b. The parameters $\delta \dot{a}_1$ and $\delta \dot{a}_2$ are respectively virtual rates of change of the two contact areas S_{b1} and S_{b2} (equal in the present isostatic simulations), and δv_{tip} is the virtual relative velocity at the tip points C and D (Fig. 2) tangential to the contact areas, measured positive if it causes an increase in the area of contact. The algebraic terms in Eqn. (10) involving γ_b and γ_p represent the power expended/released as the densification proceeds and matter having energy γ_b on the interparticle areas acquires energy γ_p when deposited on the pore surface. The mass deposited on S_p by free surface diffusion (i.e., the mass in the area bounded by S_p and the pore free surface S_p' as shown in Fig. 2) is not considered part of the particle bulk area A during its deformation process, and as such, it is not accounted for in the first integral on the right hand side of Eqn.(10). This approximation is consistent with the small displacement assumption in the model, that is, the analysis is valid for small relative density changes. However, in view of the marked effect this accumulated mass has on the pore surface curvature, the normal stress σ_n along S_p (in the third integral of the right hand side of Eqn. (10)) is related through Eqn. (8) to the curvature of the pore free surface S_p' as is configured by the deposited mass and continuously changes with time. As a result, the calculation of σ_n along S_p depends on both the particle deformation and the particle expansion α, and this couples the problem (i) for the deformation of the particle to the problem (ii) for the pore surface diffusion.

Following Needleman and Rice (1980) and Subramanian and Sofronis (2001), and using Eqs. (3), (8), and (10), and the divergence theorem, one obtains

$$\int_{S_T} T_i \delta v_i ds = \int_A \sigma_{ij} \delta \dot{\varepsilon}_{ij} dA + \int_{S_p} \gamma_p \, k \, \delta v_n ds + \int_{S_b} \frac{1}{\mathcal{D}_b} j_b \delta j_b ds + (\sigma_0 \delta j_b)_D$$
$$-(\sigma_0 \delta j_b)_C + \gamma_b \, \delta \dot{a}_1 - \gamma_p \, (\delta v_{tip} \cos\phi)_C + \gamma_b \, \delta \dot{a}_2 - \gamma_p \, (\delta v_{tip} \cos\phi)_D \, . \qquad (11)$$

By appropriate interpolations, Eqn. (11) is converted into a set of non-linear finite element equations. The contact areas BC and DE (Fig. 2), which are domains for the interparticle diffusion process, are not known beforehand and are determined as part of the solution. The overall solution strategy is incremental in time and involves assuming a size for the contact areas that is in excess of the expected. Through Newton iteration, the nonlinear finite element equations arising from Eqn. (11) are satisfied at time $t_{n+1} = t_n + \Delta t$ by solving for displacement increments $\{\Delta u\}$ using the known stresses $\{\sigma\}_n$, displacements $\{u\}_n$, and curvatures along S_p' at time t_n. Then, the contact areas are checked for

consistency, i.e., whether nodes assumed to be diffusive are indeed in contact. If this condition is not met, the assumed size of the contact areas is reduced by a node and the procedure is repeated until the solution is consistent.

(ii) the *pore surface diffusion* problem for the calculation of the expansion $\alpha(s)$: Solution to the problem (i) yields the volumetric flux j_C and j_D respectively at $s = s_C$ and $s = s_D$ (see Fig. 2) at time t_{n+1} and the coordinates $\{X\}_{n+1} = \{X\}_n + \{\Delta u\}$ of the nodes on the pore surface S_p. These pieces of information are used to integrate Eqs. (4) and (7) to obtain the expansion increments $\{\Delta\alpha\}$ such that $\{\alpha\}_{n+1} = \{\alpha\}_n + \{\Delta\alpha\}$ at time t_{n+1}, and surface S_p' is determined from $\{X\}_{n+1} + \{\alpha\}_{n+1}$. The solution to problem (ii) also provides the curvatures for the tip points C and D from which tip stresses (to be used in the solution of problem (i) at t_{n+2}) are computed through the chemical potential continuity requirement, Eqn.(9).

In summary, the solution to problem (i) enforces equilibrium in the bulk of the particle, ensures the satisfaction of the diffusion equation (3) on the interparticle boundaries BC and DE, and of the Laplace relation (8) on the pore surface S_p. The solution to problem (ii) ensures mass conservation on the pore surface as dictated by Eqn. (7), as well as enforcement of the pore surface diffusion equation (4) and chemical potential continuity at the tips C and D (Eqn. (9)).

4. DIMENSIONLESS GROUPS

The overall densification of the aggregate occurs under the simultaneous action of multiple mechanisms characterized by a large number of parameters. Therefore, in order to interpret the results of numerical computations meaningfully, it is necessary to obtain quantitative measures of the relative strengths of these mechanisms. To this end, a dimensional analysis has been performed over the geometric, material, and loading parameters leading to the following dimensionless groups (Subramanian and Sofronis, 2001):

$$\psi_b = \frac{\gamma_b}{\sigma_a R}, \quad \psi_b = \frac{\gamma_b}{\sigma_a R}, \quad \chi_b = \frac{\mathcal{D}_b}{C\sigma_a^{n-1} a^2 R}, \quad \chi_p = \frac{\mathcal{D}_p \gamma_p}{C\sigma_a^n R^4}, \tag{12}$$

where R is the particle radius, a is a characteristic size of the area (following Raj, 1974) over which interparticle diffusion occurs, and σ_a is the applied macroscopic stress (Fig. 2).

Clearly, ψ_b and ψ_p represent the strengths of the interface and pore surface tension in relation to the applied stress. The higher these values are, the larger is the energy required to be delivered by the applied loads to change the respective areas of these surfaces. Also for a given pore curvature, a higher value of ψ_p implies higher normal stresses in the adjoining bulk material.

The groups χ_b and χ_p measure respectively the strength of the interparticle and surface diffusion processes relative to the power-law creep process in the bulk. Thus, if $\chi_b = 10$ and $\chi_p = 100$, one can infer that the interparticle diffusion process was initially an order of magnitude faster than the power-law creep process and the pore surface diffusion process was two orders of magnitude faster. With regard to the interparticle diffusion length scale a, since the present study pertains to the earlier stages of densification when the size of the contacts is quite small compared to the radius of the particles, a contact size of $R/20$ has been used for a. Such a choice is in agreement with the numerical results that furnish $a < R/4$ for the range of relative densities considered.

5. THE STRAIN-RATE POTENTIAL

A convenient way to present the numerical results of the present study is by means of a potential function $\Phi(\Sigma_{ij})$ (Hill, 1967; Duva and Hutchinson, 1984; Cocks, 1989; Sofronis and McMeeking, 1992; Cocks, 1994) that is used to describe the constitutive response of the aggregate. For the problem at hand, an *admissible* stress state $[\sigma_{ij}^*, T_i^*]$ is defined to be one that (i) obeys the equilibrium equations in the bulk of the particles A, (ii) satisfies traction boundary conditions such that $T_i^* = \sigma_{ij}^* n_j$ is the traction specified on the surface S_T (n being the unit outward normal) where tractions are prescribed, and (iii) satisfies the Laplace relation $\sigma_n^* = \gamma_p k$ relating the normal stress to the curvature on S_p. On the other hand, by definition, a *kinematically admissible* state $[v_i^*, \dot{\varepsilon}_{ij}^*, j_b^*]$ is such that the velocity field v_i^* (i) possesses continuous first partial derivatives in A so that $\dot{\varepsilon}_{ij}^* = (v_{i,j}^* + v_{j,i}^*)/2$, and (ii) relates to the flux field j_b^* through the mass conservation equation (5) on S_b. For an admissible stress state $[\sigma_{ij}^*, T_i^*]$ and a kinematically admissible state $[v_i^*, \dot{\varepsilon}_{ij}^*, j_b^*]$, one can state the principle of virtual power as (Cocks, 1994)

$$\begin{aligned}\int_S T_i^* v_i^* ds = \int_A \sigma_{ij}^* \dot{\varepsilon}_{ij}^* dA + \int_{S_b} \sigma_{n,s}^* j_b^* ds + \int_{S_p} \sigma_n^* v_n^* ds + (\sigma_n^* j_b^*)_D - (\sigma_n^* j_b^*)_C \\ +\gamma_b(\dot{a}_1^* + \dot{a}_2^*) - \gamma_p\left[(v_{tip}^* \cos\phi^*)_C + (v_{tip}^* \cos\phi^*)_D\right],\end{aligned} \tag{13}$$

where $\sigma_{n,s}^*$ is the tangential gradient of the normal stress on S_b and all virtual quantities are as defined in the paragraph following Eqn. (10).

Let $[v_i^*, \dot{\varepsilon}_{ij}^*, j_b^*]$ be identified with the true state $[v_i, \dot{\varepsilon}_{ij}, j_b]$ and $[\sigma_{ij}^*, T_i^*]$ with the true state $[\sigma_{ij}, T_i]$ as the aggregate densifies under a given externally applied constant stress Σ_{ij} such that $T_i = \Sigma_{ij} n_j$ on S_T. Then, Eqn. (13) specializes to

$$\begin{aligned}\int_S T_i v_i ds = \int_A \sigma_{ij} \dot{\varepsilon}_{ij} dA + \int_{S_b} \sigma_{n,s} j_b ds + \int_{S_p} \sigma_n v_n ds + (\sigma_n j_b)_D - (\sigma_n j_b)_C \\ +\gamma_b(\dot{a}_1 + \dot{a}_2) - \gamma_p\left[(v_{tip}\cos\phi)_C + (v_{tip}\cos\phi)_D\right].\end{aligned} \tag{14}$$

Keeping the kinematic fields fixed at the true state $[v_i, \dot{\varepsilon}_{ij}, j_b]$ (i.e., under fixed particle geometry), let the external tractions be incremented by $dT_i = d\Sigma_{ij} n_j$ such that the true stresses in A are incremented by $d\sigma_{ij}$. Since no change in geometry was effected during the stress increment, the incremented stress state $[\sigma_{ij} + d\sigma_{ij}, T_i + dT_i]$ obeys exactly the same Laplace relation as the original stress state $[\sigma_{ij}, T_i]$ everywhere on the pore surface S_p, that is, $d\sigma_n = 0$ everywhere on S_p. Therefore, for the true kinematic state $[v_i, \dot{\varepsilon}_{ij}, j_b]$, and the incremented stress state $[\sigma_{ij} + d\sigma_{ij}, T_i + dT_i]$ which is clearly also an admissible stress state, the principle of virtual power (Eqn. (13)) is stated as

$$\int_S (T_i + dT_i) v_i ds = \int_A (\sigma_{ij} + d\sigma_{ij}) \dot{\varepsilon}_{ij} dA + \int_{S_b} (\sigma_{n,s} + d\sigma_{n,s}) j_b ds + \int_{S_p} \sigma_n v_n ds$$
$$+ (\sigma_n j_b)_D - (\sigma_n j_b)_C + \gamma_b (\dot{a}_1 + \dot{a}_2) - \gamma_p \left[(v_{tip} \cos\phi)_C + (v_{tip} \cos\phi)_D \right]. \quad (15)$$

Comparing Eqs. (14) and (15), one obtains the following concise relationship between the incremented stress fields and the true kinematic fields:

$$\int_S dT_i \, v_i \, ds = \int_A d\sigma_{ij} \dot{\varepsilon}_{ij} dA + \int_{S_b} d\sigma_{n.s} j_b ds \, . \quad (16)$$

Following Hill (1967), and Duva and Hutchinson (1984), we note that the left-hand side can be rewritten as

$$\int_S dT_i \, v_i \, ds = A \, d\Sigma_{ij} \dot{E}_{ij}, \quad (17)$$

where the macroscopic strain rate $\dot{E}_{ij}$ is defined through the velocities on the external boundary of the compact as $\dot{E}_{ij} = \frac{1}{2} \int_S (v_i n_j + v_j n_i) \, ds$. From Eqn. (1), it is readily seen that

$$d\sigma_{ij} \dot{\varepsilon}_{ij} = d\sigma_{ij} \frac{\partial \phi^c}{\partial \sigma_{ij}} = d\phi^c \quad (18)$$

in A. On S_b, Eqn. (3) yields

$$d\sigma_{n.s} j_b = \mathcal{D}_b \, \sigma_{n.s} d\sigma_{n.s} = d(\frac{1}{2} \mathcal{D}_b \, \sigma_{n.s}^2) = \, d\phi^b, \quad (19)$$

where ϕ^b is a potential function for interparticle diffusion (Cocks, 1994) such that

$$\phi^b = \frac{1}{2} \mathcal{D}_b \, \sigma_{n.s}^2 . \quad (20)$$

Combining Eqs. (16) through (20), one obtains the relation

$$A \, d\Sigma_{ij} \dot{E}_{ij} = d \left(\int_A \phi^c dA + \int_{S_b} \phi^b ds \right), \quad (21)$$

and hence,

$$\dot{E}_{ij} = \frac{\partial \Phi}{\partial \Sigma_{ij}}, \quad (22)$$

where

$$\Phi = \frac{1}{A}\left[\int_A \phi^c \, dA + \int_{S_b} \phi^b \, ds\right] \tag{23}$$

is the macroscopic potential for the deformation of the aggregate.

At any instant of time, the complete solution to the initial boundary value problem discussed in Section 3 yields all the information needed to numerically compute Φ. In the case of compaction under a constant macroscopic applied stress, the strain rate of the compact decreases monotonically with deformation. Hence, the macroscopic potential also varies with the deformation and it is convenient to express Φ as a function of a state variable such as the relative density of the compact. The pore surface diffusivity and pore surface energy significantly affect the flux on the contact areas as well as the stresses in the bulk of the particles, due to the coupled nature of the densification problem; so, they have an important role to play in the determination of ϕ^b and ϕ^c. Thus, although these material parameters do not explicitly appear in the above expression for Φ, it should be remembered that Φ is necessarily dependent on them.

6. NUMERICAL RESULTS

6.1. Form of the potential Φ: Computations were carried out to simulate the hydrostatic compaction of wires with a radius of 5 microns. Details of the finite element scheme employed can be found in Subramanian and Sofronis (1999, 2001). Material data used in the calculations, chosen to be those of TiAl at $625^{\circ}C$ (Ashby (1990)), are reported in Table 1. The applied stresses $\Sigma_{11} = \Sigma_{22} = -\sigma_a$ used in the computations ranged from 200 to 600 MPa, and the values of the dimensionless groups at these stresses are as shown in Table 2. Finite element computations converged extremely slowly when the creep exponent n was 3 and therefore, n was set equal to 2 in order to achieve faster convergence. However, as will be explained in the remainder of this section, since numerical computations were focussed on the case when diffusion processes dominate over power-law creep, this change of exponent did not adversely affect the computation of Φ. Finally, for the hydrostatic loading considered in this paper, the in-plane mean macroscopic stress $\Sigma_m = (\Sigma_{11} + \Sigma_{22})/2$ is equal to the applied stress σ_a.

Fig. 3 shows the variation of the normalized potential $\Phi/C\Sigma_m{}^{n+1}$ with relative density at a stress level of 400 MPa. Φ_c and Φ_b stand respectively for the contributions of the first and second integrals of Eqn. (23). Evidently, for the combination of particle size, material parameters, and applied stresses used, the contribution to Φ from the power-law creep deformation of the particles is negligible and the diffusion processes on the interparticle contacts and void surface control the overall densification behavior of the compact. This diffusion dominance was not restricted to the specific stress level of 400 MPa shown in the figure; it was observed to be the case for all the applied stresses σ_a used in the computations.

In Fig. 4, Φ is shown as a function of applied stress Σ_m at different stages of the densification. At a fixed relative density D, one observes that for the creep exponent $n = 2$ used in the present computations, the $log\left(\Phi/C\Sigma_m{}^{n+1}\right)$ vs. $log\Sigma_m$ variation is a straight line with slope of -1, i.e. $\Phi/C\Sigma_m{}^{n+1} \propto 1/\Sigma_m$. Indeed, since $\Phi \approx \Phi_b$, one expects from Eqs. (20) and (23) that $\Phi \propto \Sigma_m{}^2$, which implies that for any creep exponent n, $\Phi/C\Sigma_m{}^{n+1} \propto 1/\Sigma_m{}^{n-1}$. Since the form of stress-dependence of $\Phi/C\Sigma_m{}^{n+1}$ does not change with relative density, one can write

$$\frac{\Phi}{C\Sigma_m^{n+1}} = \frac{f(D, \text{material parameters})}{\Sigma_m^{n-1}} \,. \tag{24}$$

This simple dependence of $\Phi/C\Sigma_m^{n+1}$ on the applied stress is clearly realizable only in the regime where the diffusion processes dominate over the power-law creep process. If the first integral of Eqn. (23), which would be proportional to Σ_m^{n+1}, were at least comparable in magnitude to the second, then the form of dependence of Φ on Σ_m would be more complicated and not as straightforward to assess. However, in the case at hand, it is possible to evaluate the function f of Eqn. (24) through a systematic program of computations. For this reason, in the rest of the paper, attention will be focused on diffusion dominated densification. Of course, it is worth noting that the general formulation of Φ, as derived in the previous section, is valid for any combination of loading and material parameters.

Recalling that the dimensionless groups of Eqn. (12) depend on material and particle geometry parameters, and the applied stress Σ_m, one could rewrite Eqn. (24) in terms of dependence on χ_b, χ_p, ψ_b, and ψ_p. Specifically, $\Phi/C\Sigma_m^{n+1}$ is sought in the following form

$$\frac{\Phi}{C\Sigma_m^{n+1}} = \frac{c}{h(D)} \chi_b^{k_1} \chi_p^{k_2} \psi_p^{k_3} \psi_b^{k_4}, \tag{25}$$

where

$$h(D) = \left(\frac{D - \sqrt{D/D_0 - 1}}{D_0 - \sqrt{1 - D_0/D}} \left(1 - D_0/D\right) \right)^b, \tag{26}$$

$D_0 = \pi/4$ is the initial relative density for the square array, i.e., when the cylinders are in point contact, and b, c, k_1, k_2, k_3, and k_4 are constants to be determined. Of course, these parameters could themselves be functions of material properties and applied stresses, a scenario that is not easy to handle. Since the overall stress dependence of $\Phi/C\Sigma_m^{n+1}$ is known from Eqn. (24), the exponents k_1, k_2, k_3, and k_4 must satisfy $k_1 + 2k_2 + k_3 + k_4 = 1$. Thus, one needs to evaluate only three of the four exponents $k_i, i = 1, 4$ through computations. The specific form of $h(D)$ given in Eqn. (26) has been obtained by means of simple qualitative arguments involving the power dissipated through interparticle diffusion, and the details of this analysis are given in Appendix A.

Although Eqn. (25) has been established using real material data for TiAl compacts at $625^\circ C$, it should be noted that this equation has been cast in terms of dimensionless groups. Hence, its validity is not restricted to any single material system. In order to generalize the computation of Φ for any arbitrary material system under arbitrary loads, all computations in the remainder of the paper have been characterized simply through the dimensionless groups. It should be borne in mind that some values of the dimensionless groups used in the following case studies might not strictly correspond to the TiAl system described at the beginning of this section since they were chosen to span a wider range of material/loading combinations.

For the calculation of the parameter b, one observes that according to the suggested form of Φ (Eqn. (25)) the product $h(D)\Phi/C\Sigma_m^{n+1}$ should be independent of the relative density D for a given set of material data and applied stress. Indeed, when the exponent b was set to 1.65, the finite element results of Fig. 5 demonstrate that $h(D)\Phi/C\Sigma_m^{n+1}$ varies only slightly with D over several combinations of dimensionless groups and the entire range of relative density considered. Thus, with

the use of $b=1.65$, the present formulation reduces the description of the densification process to the determination of a single parameter, namely $h(D)\Phi/C\Sigma_m^{n+1}$ as a function of material parameters and load.

Use was made of this feature to compute the exponents k_1 through k_4 as follows: A series of computations was performed by varying the dimensionless group whose exponent was to be computed while all other dimensionless groups were kept constant. For example, in the case of k_1, the groups χ_p, ψ_b, and ψ_p were kept constant, say, at $\overline{\chi}_p$, $\overline{\psi}_b$, and $\overline{\psi}_p$ respectively, and the computations were carried out by varying χ_b. From each of these computations, $h(D)\Phi/C\Sigma_m^{n+1}$ was extracted and the numerical results were fit in the form $h(D)\Phi/C\Sigma_m^{n+1}=A\chi_b^{k_1}$ from which the exponent k_1 was read off. Of course, the fit coefficient A here is a function of the parameters $\overline{\chi}_p$, $\overline{\psi}_b$, and $\overline{\psi}_p$. The parameter c of Eqn. (25) was computed from the coefficient A of the power fit for each series, and the final value of c was taken to be the average of the values obtained from these series. The exponent k_1 was evaluated using $\chi_b=40$, 200, 2000, and 4000 while (χ_p,ψ_p,ψ_b) were fixed at $(\overline{\chi}_p,\overline{\psi}_p,\overline{\psi}_b)=(1000, 0.001, 0.0033)$, $(10000, 0.001, 0.0033)$, and $(100000, 0.001, 0.0033)$. The scalings obtained, shown in Fig. 6, led to a final value of 0.9388 for k_1. The extracted values of $h(D)\Phi/C\Sigma_m^{n+1}$ were also re-plotted against χ_p at corresponding fixed values of (χ_b,ψ_p,ψ_b) as shown in Fig. 7 and the exponent k_2 was computed to be 0.0366. Additional computations indicated that $h(D)\Phi/C\Sigma_m^{n+1}$ was completely insensitive to the value of ψ_b, and hence $k_4=0$. Lastly, the average value of c was found to be 0.00469. Thus, the final expression for the macroscopic potential is stated as

$$\frac{\Phi}{C\Sigma_m^{n+1}}=\frac{0.00469}{\left(\dfrac{D-\sqrt{D/D_0-1}}{D_0-\sqrt{1-D_0/D}}\left(1-D_0/D\right)\right)^{1.65}}\frac{\chi_b^{0.9388}\chi_p^{0.0366}}{\psi_p^{0.0120}}. \tag{27}$$

The mean macroscopic strain rate $\dot{E}_m=\left(\dot{E}_{11}+\dot{E}_{22}\right)/2$ can now be calculated from Eqn. (22) using the above expression, and the result is

$$\frac{\dot{E}_m}{C\Sigma_m^{n}}=\frac{0.00469}{\left(\dfrac{D-\sqrt{D/D_0-1}}{D_0-\sqrt{1-D_0/D}}\left(1-D_0/D\right)\right)^{1.65}}\frac{\chi_b^{0.9388}\chi_p^{0.0366}}{\psi_p^{0.0120}}. \tag{28}$$

6.2. Validation of the present model: The predictive capabilities of Eqn. (27) were evaluated using comparisons of Eqn. (28) with strain-rates obtained directly from finite element computations. Figure 8 illustrates finite element results obtained in four case studies ranging from extremely fast pore surface diffusion (circles) to slow surface diffusion (squares), and from extremely fast interparticle diffusion to moderately fast interparticle diffusion. In all the cases, the strain rates predicted by Eqn. (28) agree very well with those obtained directly from finite element calculations. The circles and squares in Fig. 8 correspond to combinations of dimensionless groups that fall well outside those

utilized in deriving Eqn. (28); remarkably, Eqn. (28) predicts the macroscopic strain rates very accurately even for these cases.

6.3. Features of the potential Φ: As densification begins with the cylinders being in point contact at relative density $D = D_0 = \pi/4$, the normal stresses on the contacts are infinite leading to infinite strain rates. Strain rates furnished by Eqn. (28) are in fact infinite at $D=D_0$, and decay rapidly with increasing relative density D. Moreover, Eqn. (28) indicates that in addition to being strongly dependent on χ_b, the macroscopic strain rate is quite sensitive to χ_p and ψ_p. The higher the value of χ_p and the lower the value of ψ_p, the higher the obtained strain rate. A stronger pore surface diffusion process means that the pore surface can absorb all the mass emanating from the interparticle contacts; a lower pore surface energy implies that pore shape changes are less expensive energetically.

The strong dependence of the strain rate $\dot{E}_m$ on relative density D is a feature shared by many of the other densification models found in the literature. Two well-known examples are the models of Kuhn and McMeeking (1992; densification occurring by power-law creep alone), and McMeeking and Kuhn (1992; densification occurring by interparticle diffusion alone), which consider compaction of aggregates of spherical particles. For the case of densification by coupled interparticle and pore-surface diffusion, Bouvard and Meister (2000) extended the two–particle model of Bouvard and McMeeking (1996) to obtain macroscopic densification rates numerically for aggregates of rigid spheres in terms of the externally applied pressure. The strain rates predicted by these models (from Eqn. (27) of Kuhn and McMeeking (1992), Eqn. (49) of McMeeking and Kuhn (1992), and Eqn. (19) of Bouvard and Meister (2000)) are shown in Fig. 9 when $n = 2$, $\psi_p = 0.001$, and $\chi_b = 40$ along with predictions of the present work. The Kuhn-McMeeking model predicts a strain rate that is an order of magnitude smaller than that of the McMeeking-Kuhn model (an inference that follows directly from the definition of χ_b), while the Bouvard-Meister result lies in between. In all these models of aggregates of spheres, the initial relative density D_0 is equal to 0.64, and at this value of D the strain rates predicted by these models is infinite, just as the present plane-strain model predicts infinite strain rate at $D = \pi/4$. The difference in D_0 employed by these three models on the one hand and the present model on the other is a direct consequence of the different geometries used; i.e., aggregates of spherical particles vs. a square array of cylinders used in the present model. Also, the Kuhn-McMeeking model completely ignores interparticle and surface diffusion; the McMeeking-Kuhn model completely ignores bulk deformation and assumes extremely fast surface diffusion; both models ignore the effects of pore surface energy. On the other hand, Eqn. (19) of Bouvard and Meister (2000) ignores surface diffusion, but includes the effect of the pore surface energy on the overall densification. For these reasons, and due to the different geometries employed, direct quantitative comparison of the results of these models to that of the present is not meaningful. However, the strain rates furnished by the present model do appear to converge to that of the diffusion-dominated densification model of McMeeking and Kuhn at relative densities greater than 0.85.

Results are also available in the literature for densification of hexagonal close-packed arrays of wires (initial density $D_0 = \pi/2\sqrt{3} \approx 0.907$). Riedel (1990) proposed a model for densification occurring under the action of interparticle diffusion alone, and Svoboda and Riedel (1995) extended this to the case of coupled grain boundary and interparticle diffusion. For $\chi_b = 40$, $\psi_p = 0.001$ and $D = 0.91$, the present model yields $\dot{E}_m/C\Sigma_m{}^n$ = 3.27, 3.56, 3.87, and 4.22 for χ_p = 10, 100, 1000, and

10000 respectively. Over this range of χ_p and for the combination of the other model parameters used, the Svoboda-Riedel model is insensitive to the value of χ_p and predicts $\dot{E}_m / C\Sigma_m^{\ n} = 2.02$, as does the Riedel model. Keeping in mind that both these models assume equilibrium-shaped pores, a feature observed only in the later stages of densification ($D > 0.91$), and therefore, that the relative density range these models pertain to is outside the range of numerical accuracy ($D < 0.9$) of the present study, the present model performs reasonably well (see Fig. 9).

7. DISCUSSION

Since a small strain approximation was adopted in the solution to the initial boundary value problem, studies were limited to changes in relative density of 5%. The constitutive law that has been derived in this paper is applicable to those regimes wherein interparticle diffusion is much faster than power-law creep deformation in the bulk of the particles. In this respect, the present model is similar to several models (McMeeking and Kuhn, 1992; Riedel, 1990, Svoboda and Riedel, 1995) already available in the literature. However, the present model accounts for the effect of surface diffusion of arbitrary strength and pore surface energy, neither of which has been dealt with in the context of densification in previous models. Numerical results (Fig. 9) indicate that the neglect of these features leads to significantly different densification rates.

The interparticle surface energy γ_b enters the variational formulation of Eqn. (11) exclusively through the algebraic terms associated with rates of growth of the contact areas. For the small values of ψ_b used (i.e. $\gamma_b / R << \sigma_a$), it is expected that these terms are negligible in comparison to the contribution from the integrals of Eqn. (11). Indeed computations indicate that the effect of γ_b on the overall deformation can be ignored, and as a consequence ψ_b is absent from Eqs. (27) and (28).

Densification data for compaction ("pressure sintering") of arrays of wires seem to be extremely scarce in the literature; in fact, the authors were not able to find any. Therefore, in order to compare the predictions of the present model with observed material behavior, one needs to turn to pressureless sintering experiments. Alexander and Balluffi (1957) studied the sintering of copper using specimens of close-packed copper wires wound around copper spools. They performed several experiments by varying the temperature and wire diameter, and tabulated the reduction in porosity as a function of time. Direct comparison of these results with those of the present model is not straightforward due to the fact that there was no externally applied stress in the experiments, whereas in the present model, densification is driven by external stresses. Therefore, one needs to extract an "equivalent external applied stress" from the sintering experiments, and this has been done as explained below.

The term 'sintering stress' has been employed in the literature (McMeeking and Kuhn, 1992; Cocks, 1994) to describe the macroscopic manifestation of the internal forces that drive sintering. Thus, for modeling purposes, the sintering stress provides an equivalent external applied stress on the aggregate; in other words, one can consider the experiments of Alexander and Balluffi to be equivalent to our model experiments occurring under an applied hydrostatic stress equal to the sintering stress. McMeeking and Kuhn (1992) have derived an expression for the sintering stress Σ_s in an aggregate of spherical particles. Following their procedure, one can obtain the sintering stress for the case of a square array of cylinders as

$$\Sigma_s = \sigma_0 \left(\frac{D - \sqrt{D/D_0 - 1}}{D_0 - \sqrt{1 - D_0/D}} \frac{D - D_0}{D} \right)^{\frac{1}{2}}, \qquad (29)$$

where $\sigma_0 = \gamma_p k_0$ is the normal stress at the junctions of the interparticle contacts and the pore surface. The term multiplying σ_0 is 0 when $D = D_0 = \pi/4$ and monotonically increases to 0.41 when $D = 0.91$. Considering that surface diffusion allows for values of k_0 that could be significantly higher than $1/R$, the initial curvature of the wires, one can reasonably deduce from Eqn. (29) that the sintering stress in the aggregate is a few multiples of γ_p/R, i.e., $\Sigma_s = \lambda \gamma_p/R$, where λ is a numerical multiplier.

Using the fact that the densification rate $\dot{D}$ is related to the macroscopic strain rate through $\dot{D}/D = -\dot{E}_{kk}$, Eqn. (28) was rewritten to yield $\dot{D}$ in terms of the dimensionless groups and the relative density D, from which D was obtained as a function of time by means of numerical integration. This procedure was repeated for different values of the multiplier λ with material parameters for copper (taken from Ashby, 1990) corresponding to $900°C$ and $1000°C$, two of the temperatures employed by Alexander and Balluffi in their experiments. (Although Alexander and Balluffi reported data for temperatures of $1050°C$ and $1075°C$ also, the particle boundaries in the aggregate disappeared fairly quickly at these temperatures. Since interparticle boundaries are assumed to persist throughout the course of densification in the present model, results of sintering at these temperatures were not employed in the comparisons.) Shown in Fig. 10 are the relative densities predicted by Eqn. (28) and those extracted from Table 1 of Alexander and Balluffi (1957). The curve for $900°C$ was obtained with an applied stress of $\sigma_a = \Sigma_m = 5\gamma_p/R$, while that for $1000°C$ was generated with $\sigma_a = \Sigma_m = 9\gamma_p/R$, and these values produced the best agreement with the experimental data amongst all those that were tried. Evidently, the present model is able to reproduce experimental observations accurately; the fact that it does so by invoking stress levels in the sintered compact that are physically very reasonable is highly encouraging and reassuring of its predictive capabilities. It is interesting to note that at the higher temperature, a larger applied stress σ_a was required to reproduce the experimental data. This is, of course, a realistic scenario: at higher temperatures, diffusion processes are faster leading to the pores being filled up faster. Consequently, the average pore radius is smaller, and by the reasoning of the previous paragraph, this translates to an increase in the equivalent stress.

8. CLOSURE

A general framework for the derivation of macroscopic constitutive potentials for powder compaction has been presented. This framework has been applied to the case of diffusion-dominated isostatic compaction of cylinders, including the effects of pore surface diffusion of arbitrary magnitude and pore surface energy. The procedure used is based on numerical computations starting from point contact between particles and studying the evolution of deformation with time while the densification mechanisms are active at the microscale. The finite element procedures for the evaluation of the potential can easily be extended to derive the corresponding constitutive potential in the presence of a strong deviatoric component in the applied stress. The derived constitutive law for the present pressure-sintering case has been found to be very sensitive to relative density (see Figs. 3 and 8); and is almost linearly dependent on the interparticle diffusion strength (Eqn. (28)). It exhibits marked dependence on the pore surface energy and the rate of the pore surface diffusion process. Lastly, it can predict quite well experimentally observed sintering data.

ACKNOWLEDGEMENT

This work was supported by the Department of Energy under grant DEFGO2-96ER45439.

Appendix A: Approximate form of the function $h(D)$

When densification is diffusion-dominated, the bulk deformation effects can be neglected and the assumption of rigid grains is valid. Hence, the normal interpenetration velocity $\dot{h}$ on the interparticle contacts is constant and consequently, the flux varies linearly on the interparticle contact (see Eqn. (5)). Then, from Eqn. (3), one finds that the normal stress varies quadratically over the contact areas (Svoboda and Riedel, 1995):

$$\frac{\sigma_n(s)}{\sigma_{max}} = g\left(\frac{s}{a}\right), \tag{A1}$$

where σ_n is the normal stress on the contact, σ_{max} is its maximum value, s is the arclength, a is the contact size, and the function g describes a parabola. Consider the case when, in addition to negligible bulk deformation effects, surface energy effects are also ignored and surface diffusion is extremely fast so as to maintain a circular pore shape at all times. Then, denoting by L the length over which the external stress $\sigma_a = \Sigma_m$ is applied, setting $s/a = \bar{s}$, writing out an overall force balance for the unit cell, and incorporating Eqn. (A1), one obtains

$$\sigma_{max} = \frac{1}{a}\frac{\Sigma_m L}{\int_0^1 g(\bar{s})\, d\bar{s}}. \tag{A2}$$

As discussed in Section 6, in the case of diffusion-dominated densification, $\Phi \approx \Phi_b$, and by virtue of Eqs. (20) and (23)

$$\Phi \propto \mathcal{D}_b \int_0^a \left(\sigma_{n,s}\right)^2 ds. \tag{A3}$$

Substitution of Eqs. (A1) and (A2) into Eqn. (A3) yields

$$\Phi \propto \frac{\mathcal{D}_b}{a^3}\left(\frac{\Sigma_m L}{\int_0^1 g(\bar{s})\, d\bar{s}}\right)^2 \int_0^1 \left(g'(\bar{s})\right)^2 d\bar{s}. \tag{A4}$$

In other words, for constant external load and material properties, the potential Φ varies as $1/a^3$. Further, from the above equation, it is also clear that the dependence of Φ on the relative density D comes through the contact size a, since all the other terms of Eqn. (A4) are independent of D. Thus, if the dependence of a on D can be established, then the function $h(D)$ of Eqn. (25) can be derived. The remainder of this Appendix is devoted to this task.

Using arguments similar to those of Arzt and coworkers (Arzt, 1982; Arzt *et al.*, 1983; Fischmeister and Arzt, 1983), we can imagine the densification process as occurring in the following sequence:

i. Initially, cylinders are in point contact, with an initial relative density $D_0 = \pi/4$, and an initial radius R_0.

ii. As the compact densifies and reaches a given relative density D, instead of letting the particle centers approach relative to one another, one can alternatively visualize the particle centers as

being fixed and that densification occurs by the particle radius increasing to R_1, leading to an overlap between particles (Fig. 11). Let the length over which the particles overlap be a_1 and θ be the angle subtended by the contact at the center of the cylinder. By geometric arguments,

$$R_1 = R_0\sqrt{D/D_0}, \qquad a_1 = R_1 \sin\theta, \tag{A5}$$

and the area of overlap S (= Area(CDE), Fig. 11) is

$$S = \frac{\theta}{2}R_1^{\,2} - \frac{1}{2}R_0 a_1. \tag{A6}$$

Combining Eqs. (A5) and (A6), one obtains

$$S = \frac{R_0^{\,2}}{2}\left[\theta\, D/D_0 - \sin\theta\sqrt{D/D_0}\right]. \tag{A7}$$

iii. The final step consists of removing the area of overlap S and redistributing it evenly over the pore surface. This further increases the radius of the pore surface to the final value R, and the contact size to the actual value a (Fig. 11). For small increases in relative density (consistent with the small strain approximation of this paper), the angle made by the final contact size at the center of the cylinder is also approximately θ. Hence, $a_1 \approx a$, and from the area of the dark shaded portion (over the pore surface) of Fig. 11

$$2S = \left(\pi/4 - \theta\right)\left(R^2 - R_1^{\,2}\right). \tag{A8}$$

From Eqs. (A5), (A7), and (A8), and using $D_0 = \pi/4$, and $\sin\theta \approx \theta$ (small angle approximation), one obtains the following expression for the radius R:

$$R = R_0\sqrt{\frac{D - \sin\theta\sqrt{D/D_0}}{D_0 - \theta}} \tag{A9}$$

The relative density D is expressed as the area fraction occupied by the particle at the end of step (iii), i.e.,

$$D = \frac{2\ \text{Area(CDO)} + \text{Area(ODF)}}{\text{Area(OCGH)}} = \frac{Ra + \left(\pi/4 - \theta\right)R^2}{\left(R\cos\theta\right)^2}, \tag{A10}$$

which can be rearranged as

$$D\left(1 - \sin^2\theta\right) = \sin\theta + D_0 - \theta. \tag{A11}$$

Since $\sin\theta \approx \theta$, the above equation gives

$$\theta = \sqrt{\frac{D - D_0}{D}}, \tag{A12}$$

which when inserted in Eqn. (A9) yields

$$R = R_0\sqrt{\frac{D - \sqrt{\left(D/D_0\right) - 1}}{D_0 - \sqrt{1 - \left(D_0/D\right)}}}. \tag{A13}$$

Since $a = R\sin\theta \approx R\theta$, the required relationship between a and D is obtained through using (A12) and (A13)

$$a = R_0\left(\frac{D-\sqrt{D/D_0-1}}{D_0-\sqrt{1-D_0/D}}\left(1-D_0/D\right)\right)^{\frac{1}{2}}. \qquad \text{(A14)}$$

Recalling from Eqn. (A4) that $\Phi \propto 1/a^3$, one concludes from (A14) that

$$h(D) = \left(\frac{D-\sqrt{D/D_0-1}}{D_0-\sqrt{1-D_0/D}}\left(1-D_0/D\right)\right)^{\frac{3}{2}}, \qquad \text{(A15)}$$

for the case of extremely fast surface diffusion with no surface energy effects. For the more general case of arbitrarily fast surface diffusion and significant surface energy effects, the assumption is made that $h(D)$ is of the same form except that instead of the exponent of $3/2$ an exponent b is used, and the specific choice of this exponent is made as described in Section 6.

REFERENCES

Abouaf, M., Chenot, J. L., Raisson, G., and Bauduin, P., 1988. Finite element simulation of hot isostatic pressing of metal powders. *Int. J. Num. Meth. Engg.* 25 (1), 191-212.

Akisanya, A. R. and Cocks, A. C. F., 1995. Stage I compaction of cylindrical particles under non-hydrostatic loading. *J. Mech. Phys. Solids* 43 (4), 605-636.

Akisanya, A. R., Cocks, A. C. F. and Fleck, N. A., 1994. Hydrostatic compaction of cylindrical particles. *J. Mech. Phys. Solids* 42 (7), 1067-1085.

Alexander, B. H., and Balluffi, R. W., 1957. The mechanism of sintering of copper. *Acta Metal.* 5 (11), 666-677.

Arzt, E., 1982. The influence of an increasing particle coordination on the densification of spherical powders. *Acta Metal.* 30 (10), 1883-1890.

Arzt, E., Ashby, M. F. and Easterling, K. E., 1983. Practical applications of hot-isostatic pressing diagrams: Four case studies. *Metal. Trans.* 14A (2), 211-221.

Ashby, M. F., 1974. A first report on sintering diagrams. *Acta Metal.* 22 (3), 275-289.

Ashby, M. F., 1990. HIP 6.0 User Manual.

Bouvard, D., and McMeeking, R. M., 1996. The deformation of interparticle necks by diffusion controlled creep. *J. Am. Cer. Soc.* 79 (3), 666-672.

Bouvard, D., and Meister, T., 2000. Modelling bulk viscosity of powder aggregate during sintering. *Mod. Sim. Mater. Sci.*. 8 (3), 377-388.

Chuang, T.-Z., Kagawa, I. K., Rice, J. R., and Sills, L. B., 1979. Non-equilibrium models for diffusive cavitation of grain interfaces. *Acta Metal.* 27 (3), 265-284.

Cocks, A. C. F., 1989. Inelastic deformation of porous materials. *J. Mech. Phys. Solids* 37 (6), 693-715.

Cocks, A. C. F., 1994. The structure of constitutive laws for the sintering of fine-grained materials. *Acta Metal. Mater.* 42 (7), 2191-2210.

Cocks, A. C. F., and Aparicio, N. D., 1994. Diffusional creep and sintering - the application of bounding theorems. *Acta Metal. Mater.* 43 (2), 731-741.

Duva, J. M., 1986. A constitutive description of nonlinear materials containing voids. *Mech. Mater.* 5 (2), 137-144.

Duva, J. M., and Hutchinson, J. W., 1984. Constitutive potentials for dilutely voided nonlinear materials. *Mech. Mater.* 3 (1), 41-54.

Fishcmeister, H. F. and Arzt, E., 1983. Densification of powders by particle deformation. *Pow. Metal.* 26 (2), 82-88.

Fleck, N. A., 1995. On the cold compaction of powders. *J. Mech. Phys. Solids*, 43 (9), 1409- 1431.

Fleck, N. A., Kuhn, L. T. and McMeeking, R. M., 1992. Yielding of metal powder bonded by isolated contacts. *J. Mech. Phys. Solids*, 40 (5), 1139-1162.

Freund, L. B., Beltz, G. E., and Jonsdottir, F., 1993. Continuum modeling of stress-driven surface diffusion in strained elastic materials. *Mat. Res. Soc. Symp. Proc.* 308, 383-394.

Govindarajan, R. M., and Aravas, N., 1994a. Deformation processing of metal powders: Part I - cold isostatic pressing. *Int. J. Mech. Sci.* 36 (4), 343-357.

Govindarajan, R. M., and Aravas, N., 1994b. Deformation processing of metal powders: Part II - hot isostatic pressing. *Int. J. Mech. Sci.* 36 (4), 359-372.

Guennouni, T., and Francois, D., 1987. Constitutive equations for rigid plastic or viscoplastic materials containing voids. *Fatigue Fract. Engg. Mater. Struct.*, 10 (5), 399-418.

Guennouni, T., and Francois, D., 1988. Influence of the pore morphology and secondary cavities on the plastic behavior of porous materials. *Fatigue Fract. Engg. Mater. Struct.*, 11 (4), 267-276.

Gurson, A. L., 1977. Continuum theory of ductile rupture by void nucleation and growth: Part I - yield criteria and flow rules for porous ductile media, *J. Engg Mater. Tech., Trans. ASME*, 99 (1), 2-15.

Gurtin, M. E. and Murdoch, A. I., 1975. A continuum theory of elastic material surfaces. *Arch. Rat. Mech. Anal.* 57 (4), 291-323.

Helle, A. S., Easterling, K. E. and Ashby, M. F., 1985. Hot-isostatic pressing diagrams: New developments. *Acta Metal.* 33 (12), 2163-2174.

Herring, C., 1951. Surface tension as a motivation for sintering. In: The Physics of Powder Metallurgy - A symposium held at Bayside, L. I., New York, August 24-26, 1949, pp 143-179.

Hill, R., 1967. The essential structure of constitutive laws for metal composites and polycrystals. *J. Mech. Phys. Solids.* 15 (1), 79-95.

Kailasam, M., and Ponte Castaneda, P., 1996. Constitutive relations for porous materials: the effect of changing void shape and orientation, IUTAM Symposium on Micromechanics of Plasticity and Damage of Multiphase Materials, (eds. A. Pineau and A. Zaoui), pp. 215-222.

Kailasam, M., Aravas, N., and Ponte Castaneda, P., 2000. Porous metals with developing anisotropy: constitutive models, computational issues and applications to deformation processing. *CMES*, 1 (2), 105-118.

Kim K. T., Kim, H. G., and Jang, H. M., 1998. Densification behavior and grain growth of zirconia powder compact under high temperature. *Int. J. Engg. Sci.* 36 (11), 1295-1312.

Kuhn, L. T. and McMeeking, R. M., 1992. Power law creep of powder bonded by isolated contacts. *Intl. J. Mech. Sci.* 34 (7), 563-573.

Leblond, J. B., Perrin, G., and Suquet, P., 1994. Exact results and approximate models for porous viscoplastic solids. *Intl. J. Plast.* 10 (3), 213-235.

Leblond, J. B., Perrin, G., and Deveaux, J., 1995. An improved Gurson-type model for hardenable ductile metals. *Eur. J. Mech. A/Solids.* 14 (4), 499-527.

McMeeking, R. M. and Kuhn, L. T., 1992. A diffusional creep law for powder compacts. *Acta Metal. Mater.* 40 (5), 961-969.

McMeeking, R. M., 1992. Constitutive laws for sintering and pressing of powders, In: Mechanics of granular materials and powder systems. ASME AMD, Vol. 37, pp. 51-61, New York, NY.

Needleman, A. and Rice, J. R., 1980. Plastic creep flow effects in the diffusive cavitation of grain boundaries. *Acta Metal.* 28 (10), 1315-1332.

Ponte Castaneda, P., and Willis, J. R., 1988. On the overall properties of nonlinearly viscous composites. *Proc. Roy. Soc. Lond.* A 416 (1850), 217-244.

Ponte Castaneda, P., and Zaidman, M., 1994. Constitutive models for porous materials with evolving microstructure. *J. Mech. Phys. Solids.* 42 (9) 1459-1497.

Ponte Castaneda, P., 1997. Nonlinear composite materials: effective constitutive behavior and microstructure evolution. In *Continuum Micromechanics, CISM Courses and Lectures No. 377.* Ed. P. Suquet, Springer-Verlag, Vienna, pp. 131-195.

Ponte Castaneda, P., and Suquet, P., 1998. Nonlinear composites. *Advances in Applied Mechanics.* 34, 171-302.

Raj, R., 1974. Transient behavior of diffusion-induced creep and creep rupture. *Met. Trans. A* . 6A (8), 1499-1509.

Rice, J. R. and Chuang, T.-J., 1981. Energy variations in diffusive cavity growth. *J. Am. Cer. Soc.* 64 (1), 46-53.

Riedel, H. 1990. A constitutive model for the finite-element simulation of sintering - distortions and stresses. In: *Ceramic Transactions, Ceramic Powder Science III* (eds. G. L. Messing, S.-I. Hirano and H. Hausner), Vol. 12, pp. 619-630, Westerville, Ohio.

Schafrik, R. E., 1977. Dynamic elastic moduli of the Titanium Aluminides. *Metal. Trans.* 8A (6), 1003-1006.

Sofronis, P., and McMeeking, R. M., 1992. Creep of power-law material containing spherical voids. *J. Appl. Mech.* 59 (2), 88-95.

Storakers, B., Fleck, N. A., and McMeeking, R. M., 1999. The viscoplastic compaction of composite powders. *J. Mech. Phys. Solids* 47 (4), 785-815.

Subramanian, S. J. and Sofronis, P., 1999. Modeling of the interaction between densification mechanisms in powder compaction. University of Illinois at Urbana-Champaign, TAM Report No. 907, May 1999.

Subramanian, S. J., and Sofronis, P., 2001. Modeling the interaction between densification mechanisms in powder compaction. To appear in the *International Journal of Solids and Structures.*

Svoboda, J., and Riedel, H., 1995. Quasi-equilibrium sintering for coupled grain-boundary and surface diffusion. *Acta Metal. Mater.* 43 (2), 499-506.

Swinkels, F. B., and Ashby, M. F., 1981. A second report on sintering diagrams. *Acta Metal.* 29 (2), 259-281.

TABLE 1: Material properties for γ-*TiAl* (Ashby, 1990).

Surface energy $\gamma_p = 1.76$ J/m^2

Atomic Volume $\Omega = 3.11\times10^{-29}$ m^3

Melting point $T_m = 1730$ K

Young's modulus $E = 153$ GPa[a] at 625°C

Poisson's ratio $\nu = 0.24$[a]

Power-law creep: $\dot{\varepsilon} = D_c\left(\frac{\sigma}{\sigma_{ref}}\right)^n$, $D_c = 10^{-6}\exp[\frac{-Q_c}{RT_m}(\frac{T_m}{T}-2)]$

Activation energy $Q_c = 320.0$ kJ/mol

Power-law creep exponent $n = 2$[b]

Reference Stress $\sigma_{ref} = 1800$ MPa

Grain boundary diffusion: $D_b\delta_b = D_{0b}\delta_{0b}\exp(-\frac{Q_b}{RT})$

Activation energy $Q_b = 180.0$ kJ/mol

Pre-exponential $D_{0b}\delta_0 = 7.6\times10^{-13}$m^3/s

Surface diffusion: $D_p\delta_p = D_{0p}\delta_{0p}\exp(-\frac{Q_p}{RT})$

Activation energy $Q_p = 150.0$ kJ/mol

Pre-exponential $D_{0p}\delta_{0p} = 7.6\times10^{-10}$m^3/s

[a] Estimated from Schafrik (1977).

[b] Changed from 3 to 2 for faster convergence of the numerical scheme

TABLE 2: Values of the dimensionless groups for γ-TiAl powder at $625^{\circ}C$

Σ_m(MPa)	χ_b	χ_p	ψ_p	ψ_b
100	1303.4	637.8	0.00352	0.00117
200	651.7	159.48	0.00176	0.00058
250	521.4	102.08	0.00141	0.00047
300	434.5	70.9	0.00117	0.00039
350	372.4	52.1	0.00101	0.00034
400	325.9	39.9	0.00088	0.00029
450	289.6	31.5	0.00078	0.00026
500	260.7	25.5	0.00070	0.00023
550	237.0	21.1	0.00064	0.00021
600	217.2	17.7	0.00059	0.00020

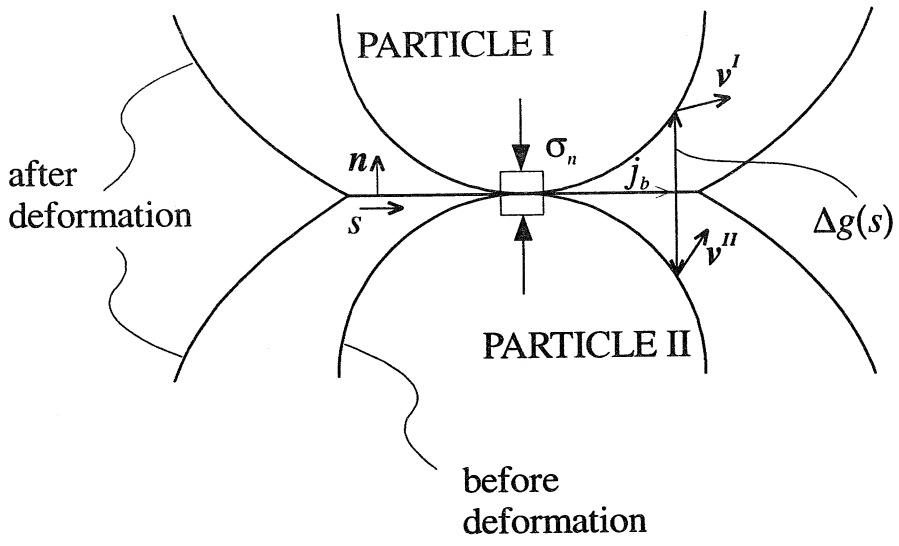

Figure 1a. The interparticle contact area: s is the arclength, **n** is the unit normal vector, σ_n is the normal stress, j_b is the volumetric flux and $\Delta g(s)$ is the non-negative gap function.

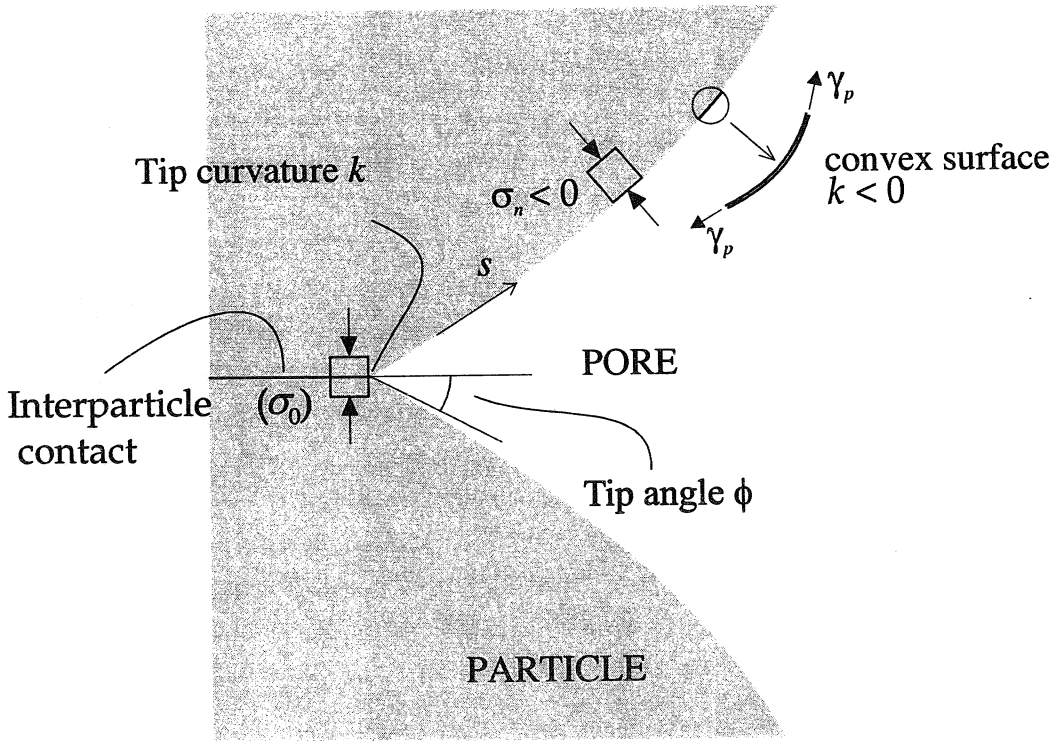

Figure 1b. Sign convention for curvature on the pore surface: k is negative if the center of curvature is in the region occupied by the particle (pore is concave) and correspondingly the stress is compressive.

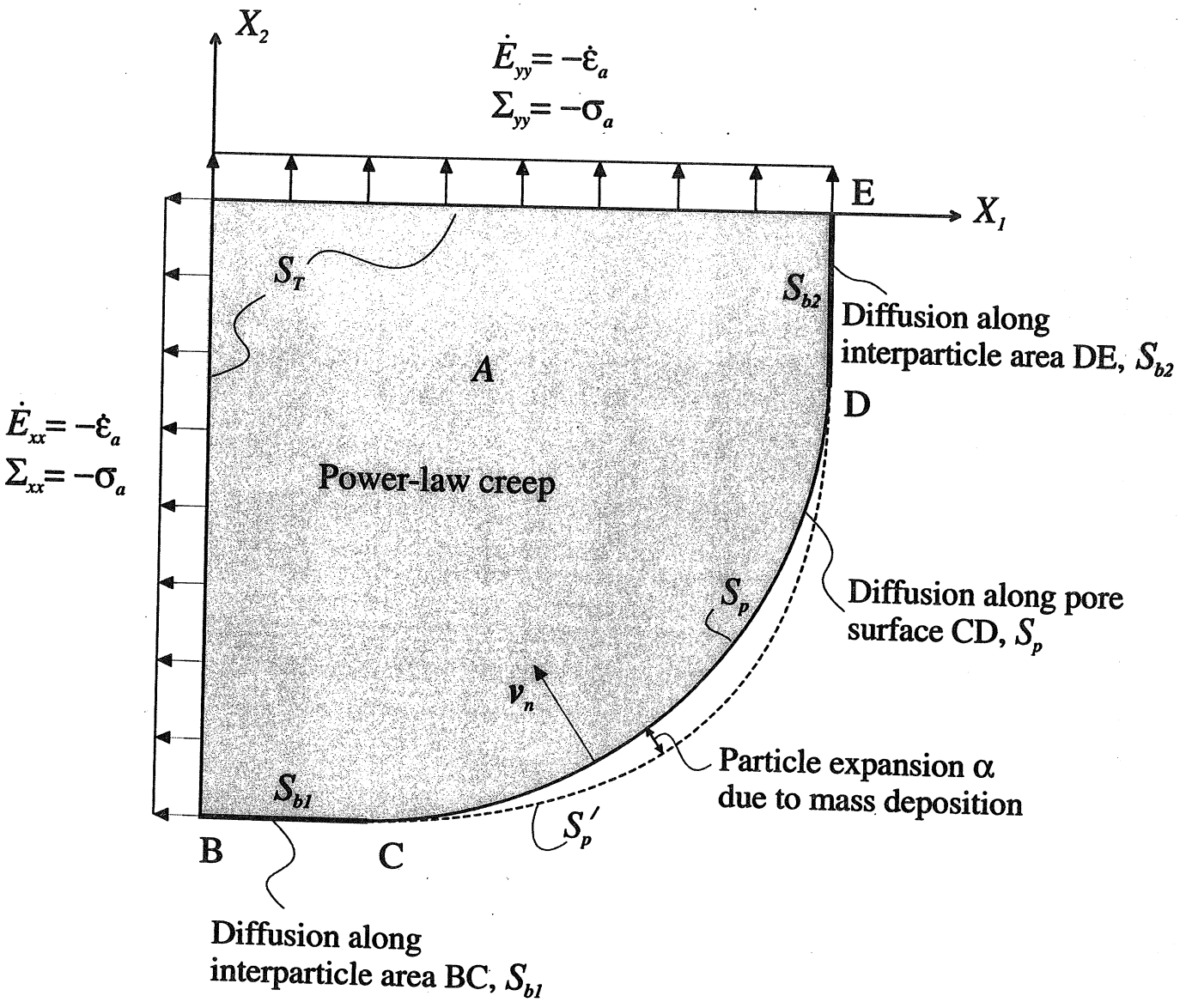

Figure 2. Definition of the domain and boundary conditions for the unit cell.

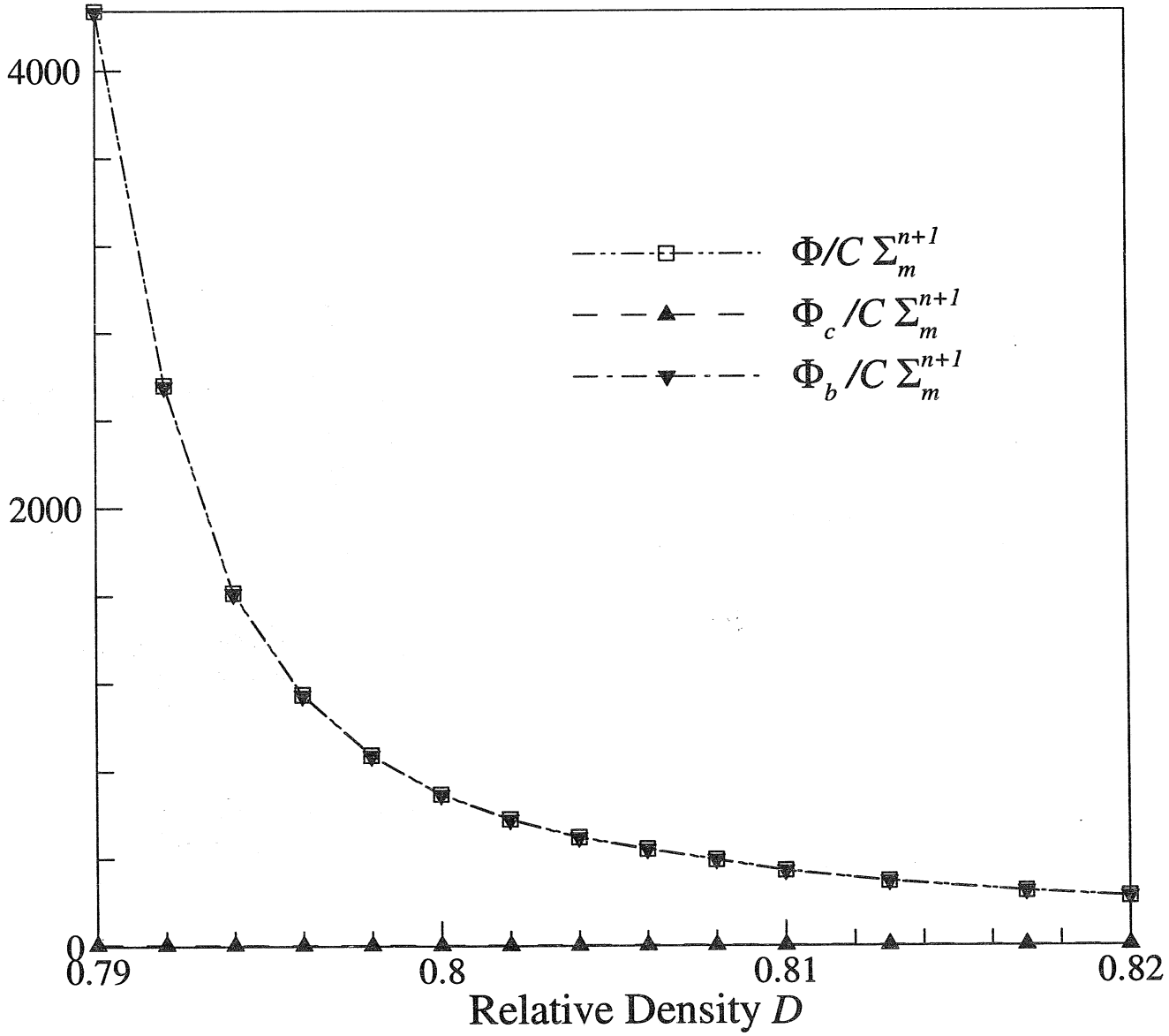

Figure 3. The normalized potential $\Phi/C\Sigma_m{}^{n+1}$, $(n=2)$, as a function of relative density, in the case of diffusion-dominated densification of TiAl at $625^{\circ}C$ under a stress of 400 MPa. $\Phi_b = \frac{1}{A}\int_{S_b}\frac{1}{2}\mathcal{D}_b\,\sigma_{n.s}^2\,ds$ and $\Phi_c = \frac{1}{A}\int_A \frac{1}{n+1}\sigma_{ij}\dot{\varepsilon}_{ij}dA = \Phi - \Phi_b$.

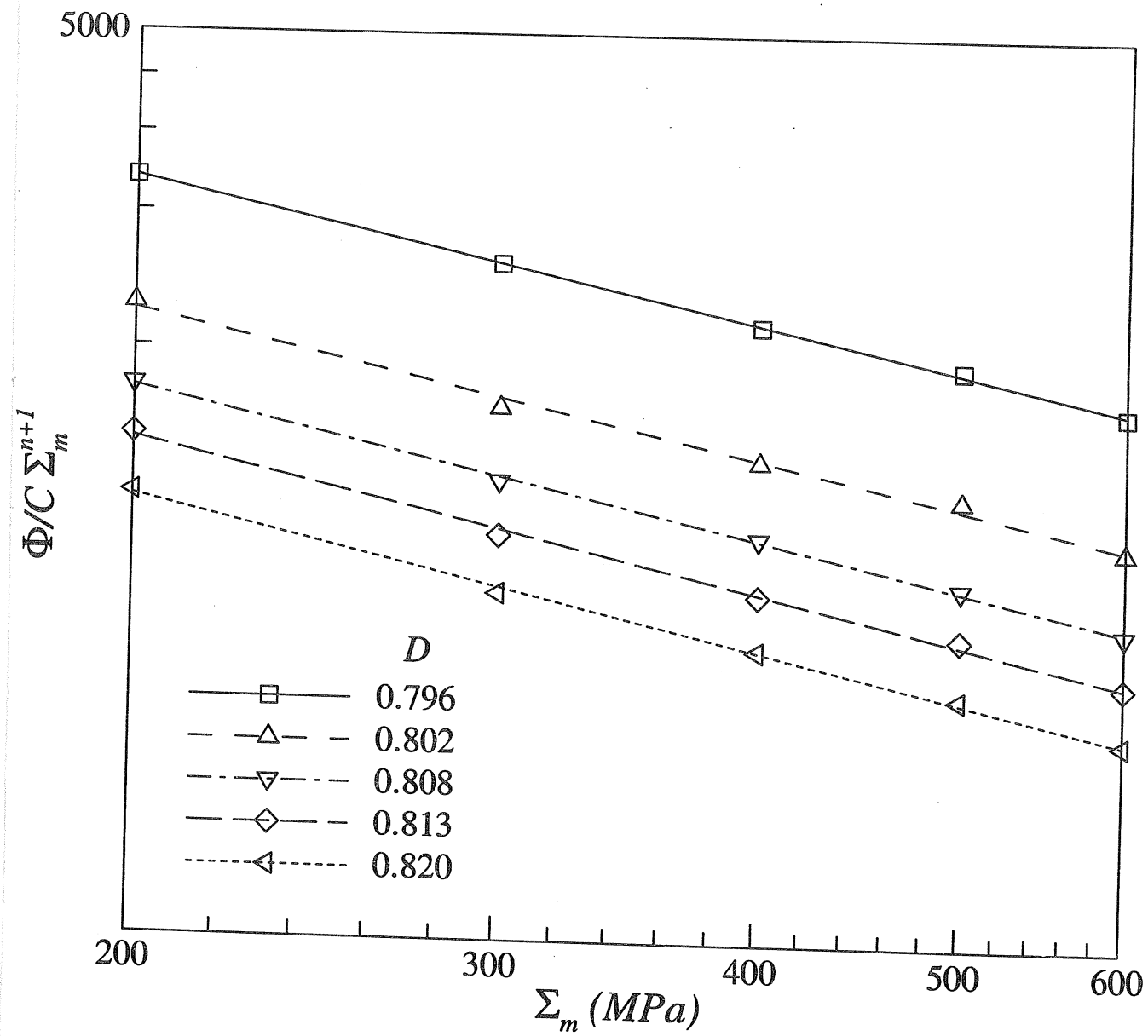

Figure 4. Scaling of $\Phi/C\Sigma_m^{n+1}$ with applied stress at constant relative density in the case of densification of TiAl at $625^{\circ}C$ dominated by diffusion with $n=2$.

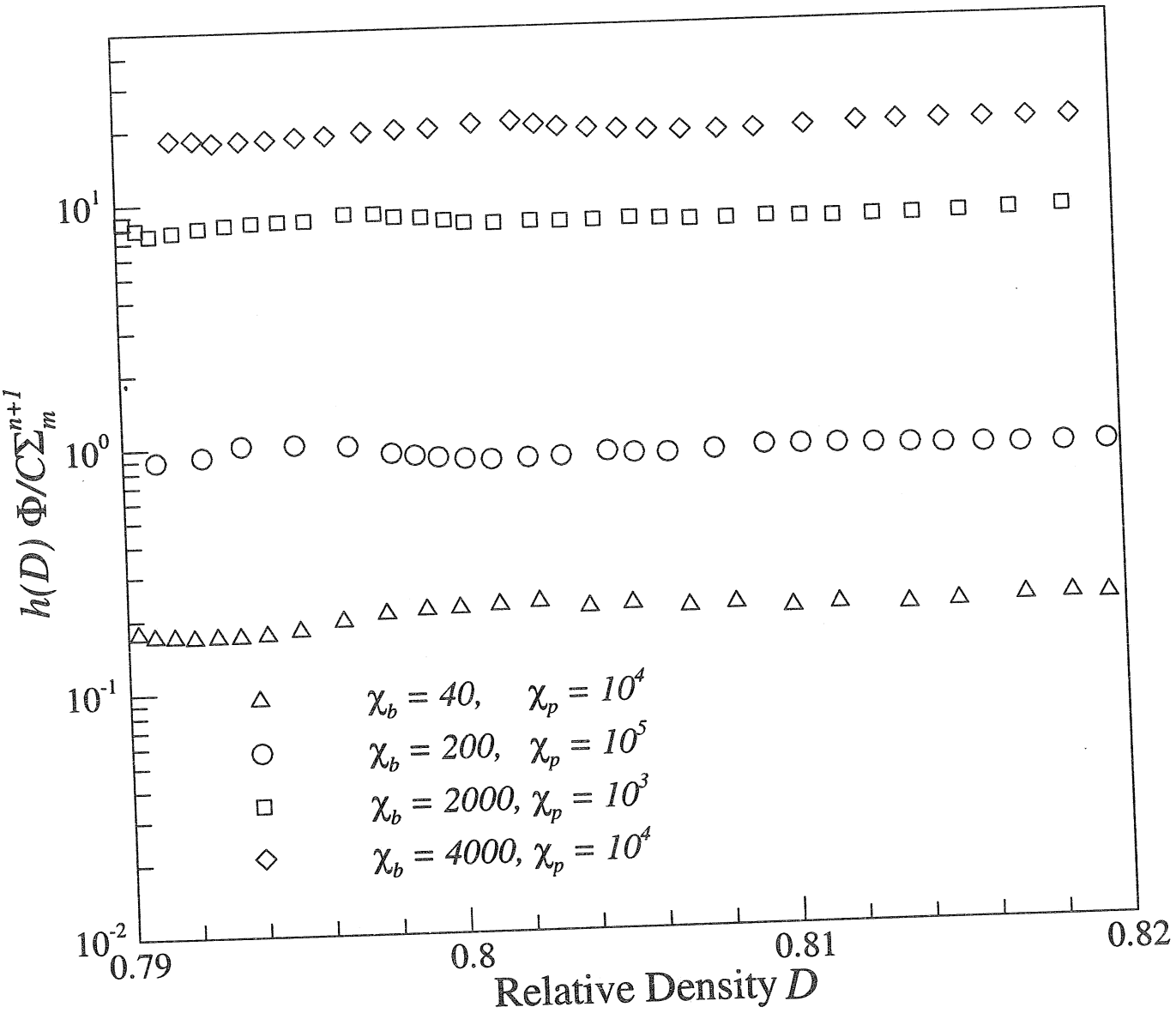

Figure 5. Variation of $h(D)\Phi/C\Sigma_m^{n+1}$ with relative density: $\psi_p = 0.001$, $\psi_b = 0.00033$, and $b = 1.65$ for all cases shown.

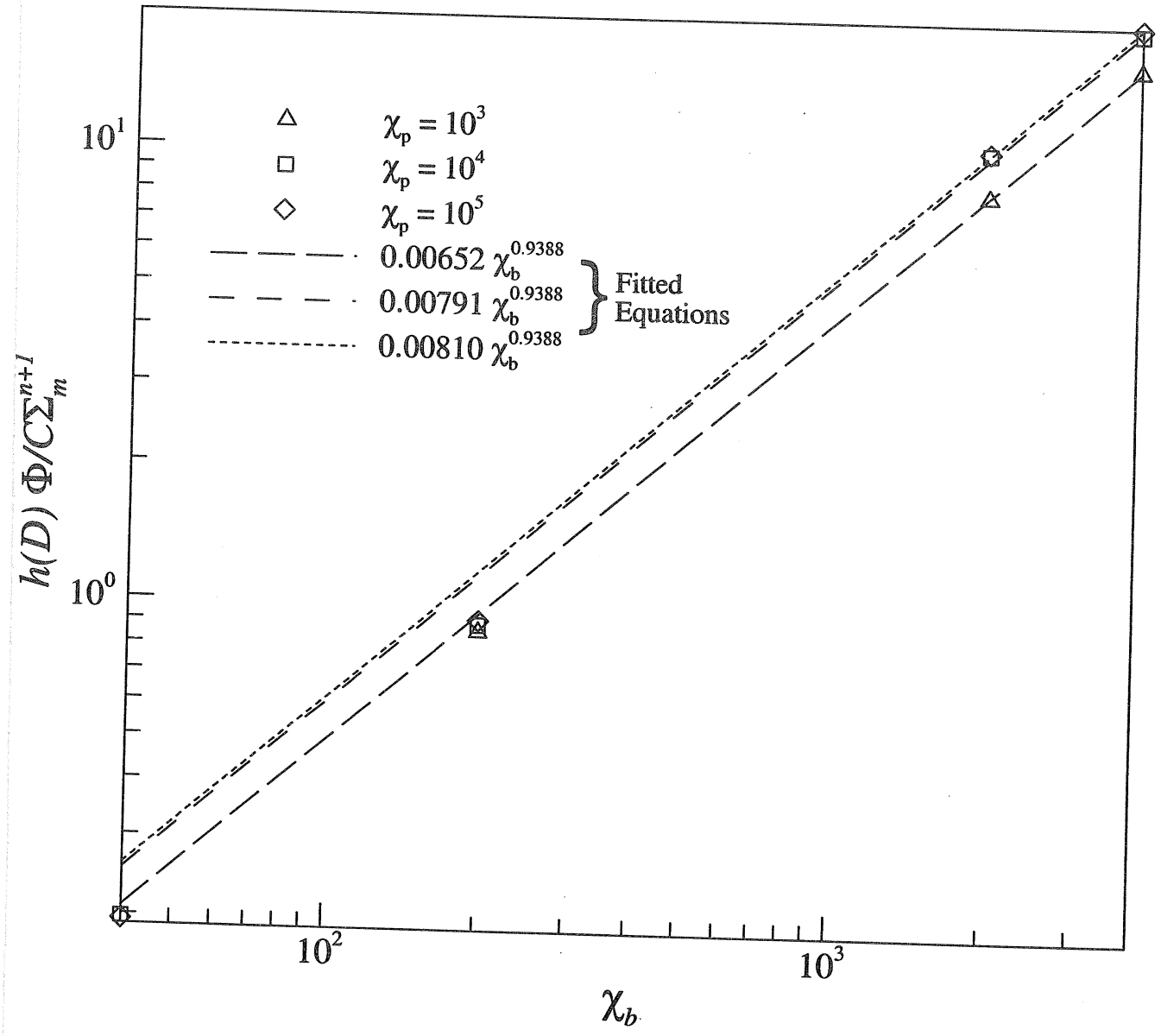

Figure 6. Scaling of $h(D)\Phi/C\Sigma_m{}^{n+1}$ with the interparticle diffusion parameter χ_b at different fixed values of χ_p: $\psi_p = 0.001$, and $\psi_b = 0.00033$.

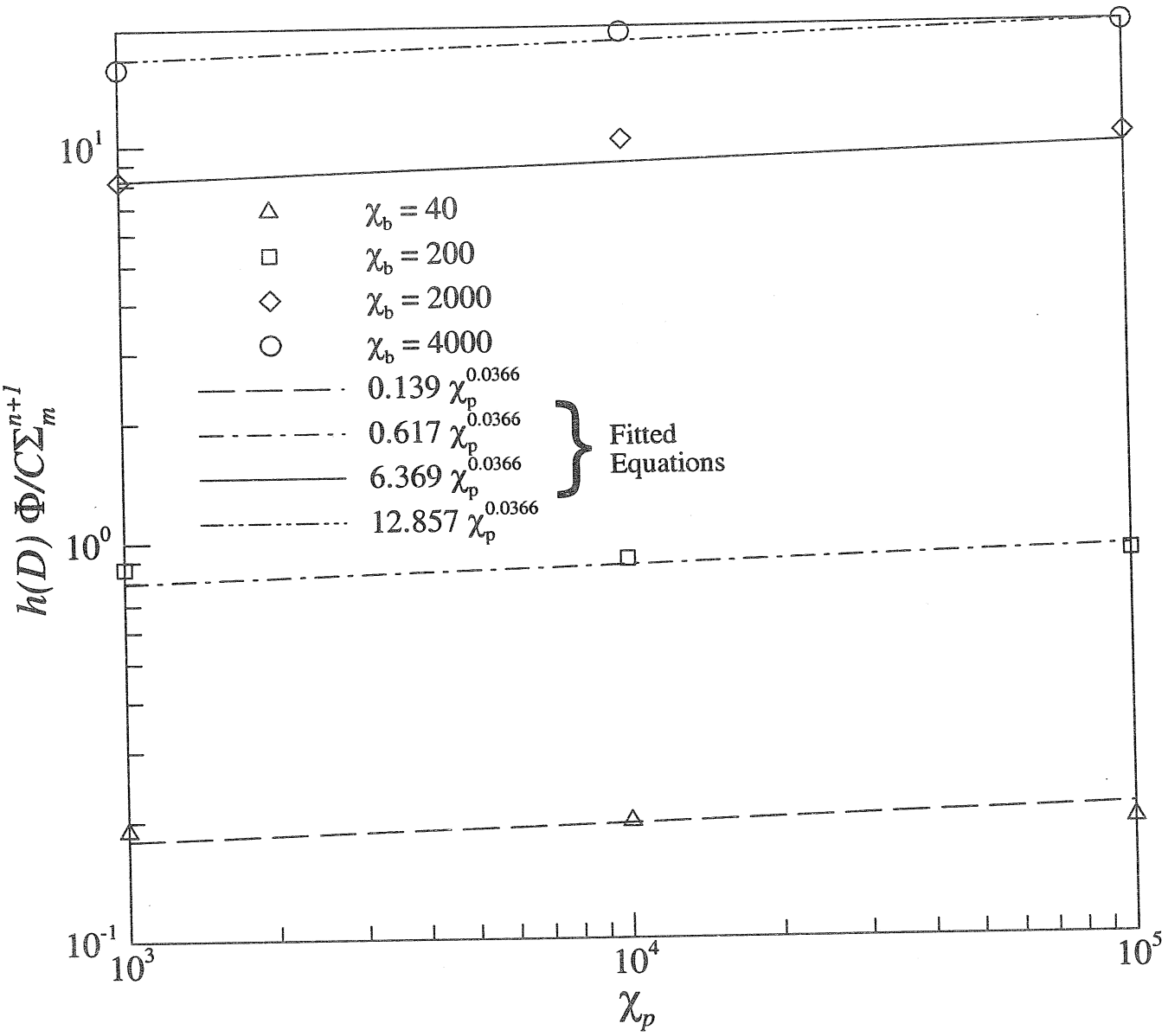

Figure 7. Scaling of $h(D)\Phi/C\Sigma_m^{n+1}$ with the pore surface diffusion parameter χ_p at different fixed values of χ_b: $\psi_p = 0.001$, and $\psi_b = 0.00033$.

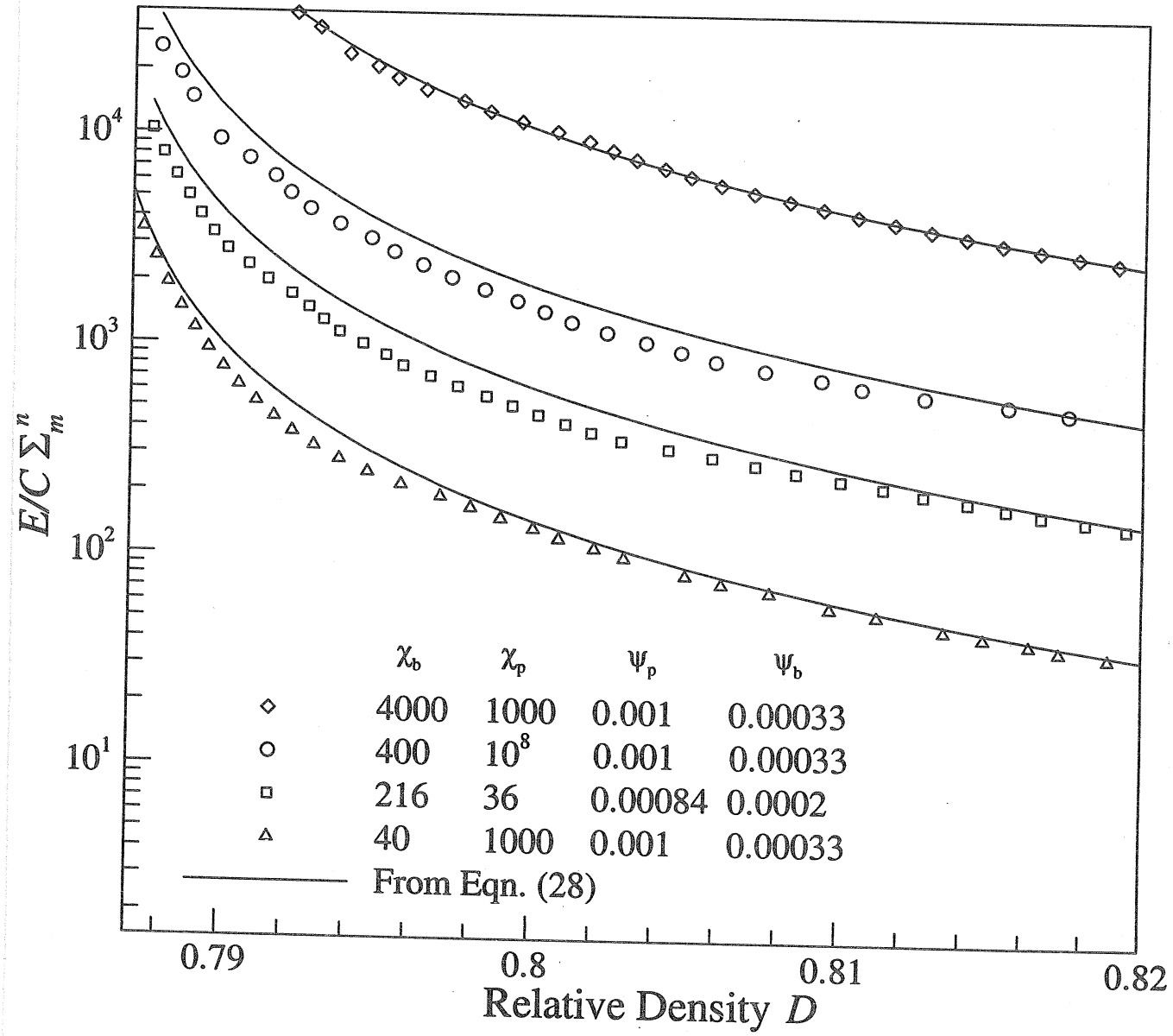

Figure 8. Comparison of strain rates predicted using Eqn. (28) (solid lines) and those obtained directly from finite element calculations (data points).

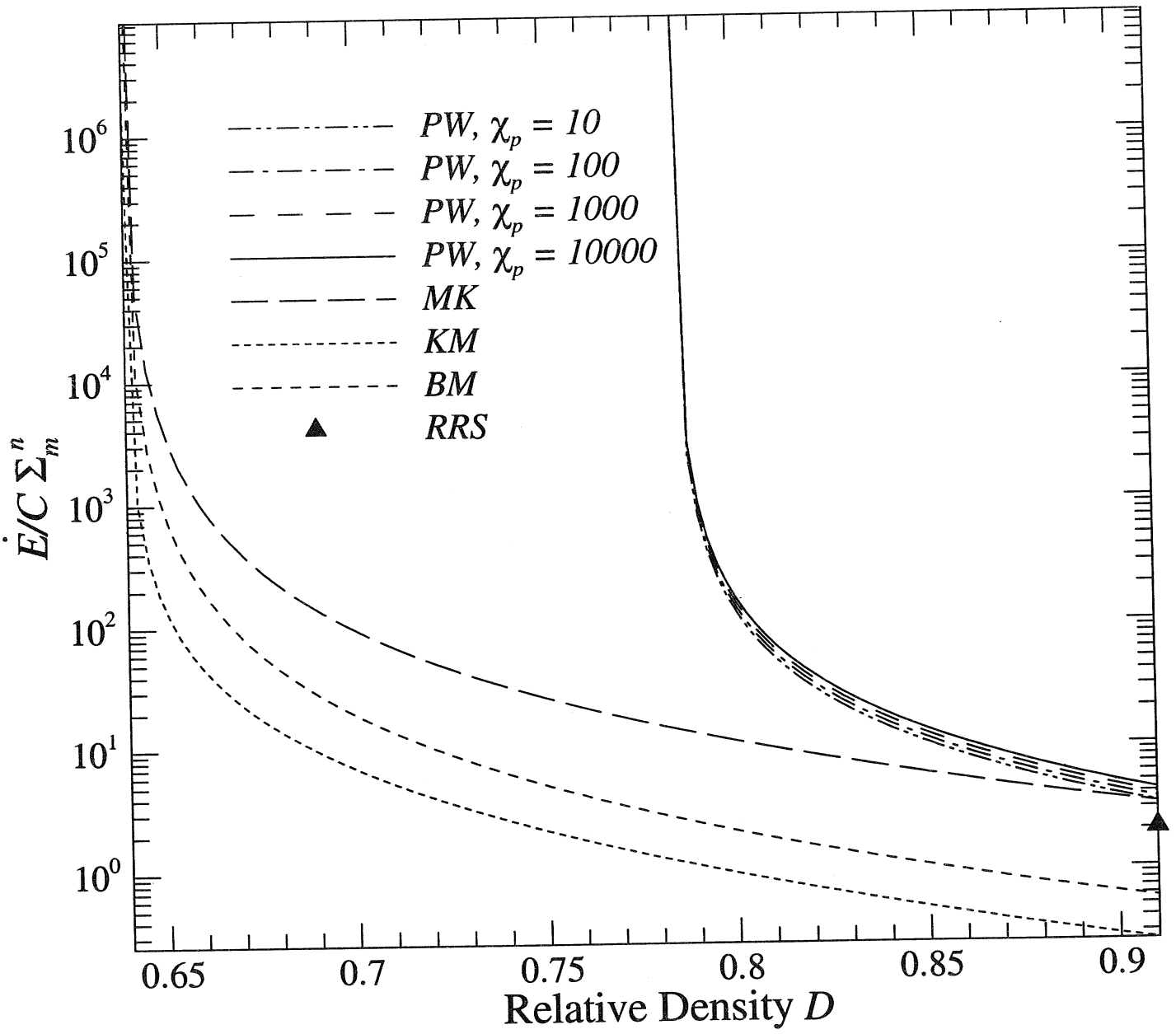

Figure 9. Macroscopic strain rate predictions of the present work (PW) along with predictions from spherical particle aggregate models. MK refers to the interparticle diffusion model of McMeeking and Kuhn (1992), KM to the power-law creep model of Kuhn and McMeeking (1992), BM to the coupled interparticle and surface diffusion model of Bouvard and Meister (2000), and RRS to the models of Riedel (1990), and Svoboda and Riedel (1995).

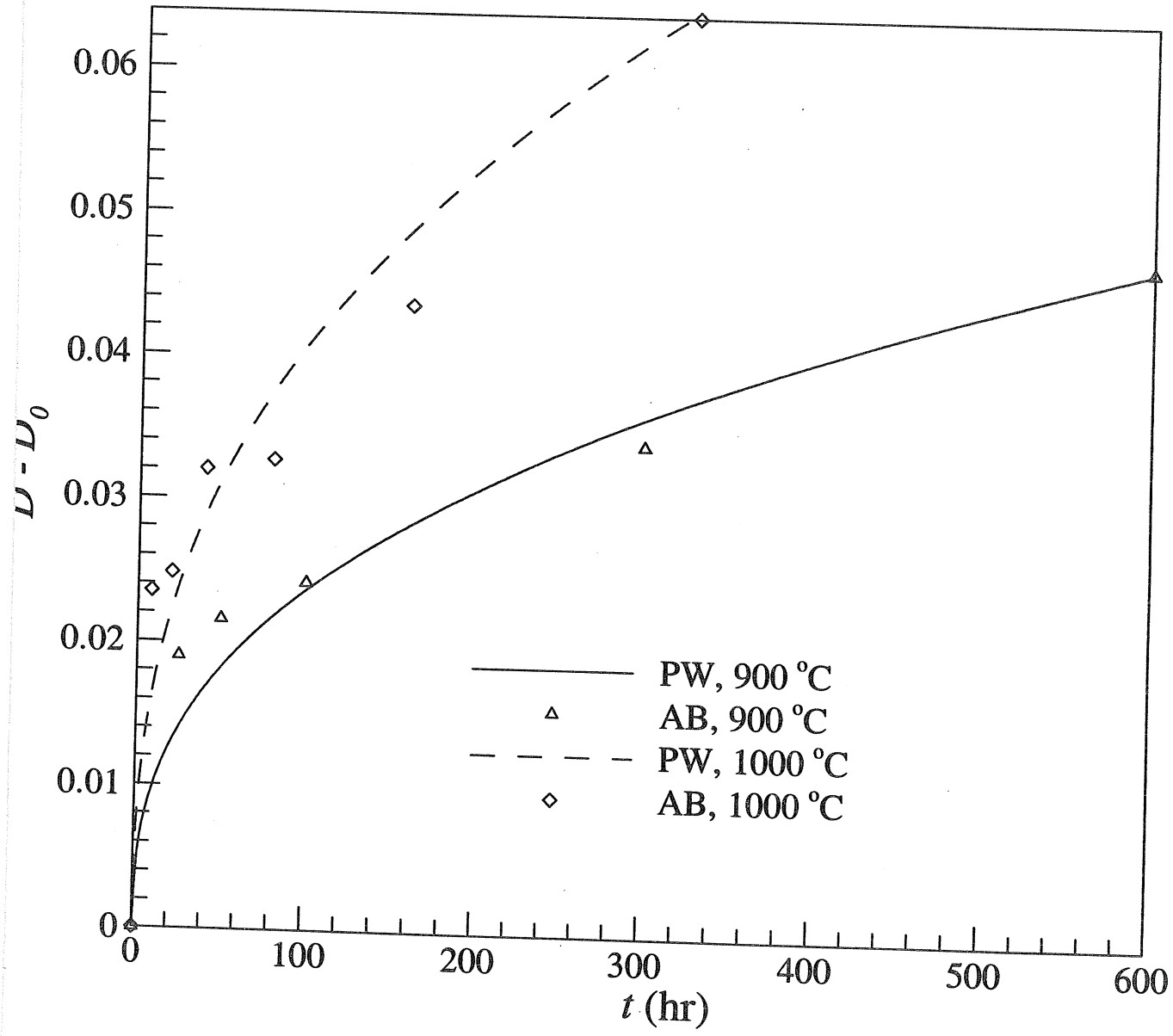

Figure 10. Comparison of relative densities derived from Eqn. (28) with those of experiments of Alexander and Balluffi on sintering of copper wires. PW refers to predictions of the present work, and AB to experimental data from Alexander and Balluffi (1957).

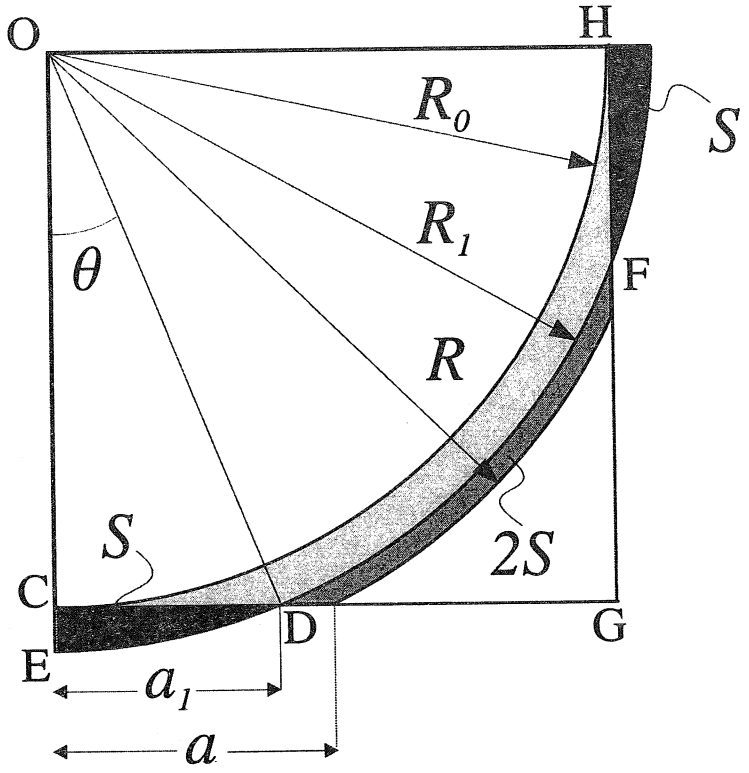

Figure 11. Sequence of steps in the visualization of the densification process: R_0 is the initial undeformed radius; R_1 and a_1 are respectively an intermediate radius of the pore surface and contact length; R and a are the radius of the pore surface and contact area respectively when the relative density is D

List of Recent TAM Reports

No.	Authors	Title	Date
888	Fried, E., and S. Sellers	The Debye theory of rotary diffusion—*Archive for Rational Mechanics and Analysis* **158**, 1–27 (2001)	Sept. 1998
889	Short, M., A. K. Kapila, and J. J. Quirk	The hydrodynamic mechanisms of pulsating detonation wave instability—*Proceedings of the Royal Society of London, A* **357**, 3621–3638 (1999)	Sept. 1998
890	Stewart, D. S.	The shock dynamics of multidimensional condensed and gas phase detonations—Proceedings of the 27th International Symposium on Combustion (Boulder, Colo.)	Sept. 1998
891	Kim, K. C., and R. J. Adrian	Very large-scale motion in the outer layer—*Physics of Fluids* **2**, 417–422 (1999)	Oct. 1998
892	Fujisawa, N., and R. J. Adrian	Three-dimensional temperature measurement in turbulent thermal convection by extended range scanning liquid crystal thermometry—*Journal of Visualization* **1**, 355–364 (1999)	Oct. 1998
893	Shen, A. Q., E. Fried, and S. T. Thoroddsen	Is segregation-by-particle-type a generic mechanism underlying finger formation at fronts of flowing granular media?—*Particulate Science and Technology* **17**, 141–148 (1999)	Oct. 1998
894	Shen, A. Q.	Mathematical and analog modeling of lava dome growth	Oct. 1998
895	Buckmaster, J. D., and M. Short	Cellular instabilities, sub-limit structures, and edge-flames in premixed counterflows—*Combustion Theory and Modeling* **3**, 199–214 (1999)	Oct. 1998
896	Harris, J. G.	*Elastic waves*—Part of a book to be published by Cambridge University Press	Dec. 1998
897	Paris, A. J., and G. A. Costello	Cord composite cylindrical shells	Dec. 1998
898	Students in TAM 293–294	Thirty-fourth student symposium on engineering mechanics (May 1997), J. W. Phillips, coordinator: Selected senior projects by M. R. Bracki, A. K. Davis, J. A. (Myers) Hommema, and P. D. Pattillo	Dec. 1998
899	Taha, A., and P. Sofronis	A micromechanics approach to the study of hydrogen transport and embrittlement—*Engineering Fracture Mechanics*, in press (2001)	Jan. 1999
900	Ferney, B. D., and K. J. Hsia	The influence of multiple slip systems on the brittle–ductile transition in silicon—*Materials Science Engineering A* **272**, 422–430 (1999)	Feb. 1999
901	Fried, E., and A. Q. Shen	Supplemental relations at a phase interface across which the velocity and temperature jump—*Continuum Mechanics and Thermodynamics* **11**, 277–296 (1999)	Mar. 1999
902	Paris, A. J., and G. A. Costello	Cord composite cylindrical shells: Multiple layers of cords at various angles to the shell axis—*Journal of Applied Mechanics* **67**, 117–127 (2000)	Apr. 1999
903	Ferney, B. D., M. R. DeVary, K. J. Hsia, and A. Needleman	Oscillatory crack growth in glass—*Scripta Materialia* **41**, 275–281 (1999)	Apr. 1999
904	Fried, E., and S. Sellers	Microforces and the theory of solute transport—*Zeitschrift für angewandte Mathematik und Physik* **51**, 732–751 (2000)	Apr. 1999
905	Balachandar, S., J. D. Buckmaster, and M. Short	The generation of axial vorticity in solid-propellant rocket-motor flows—*Journal of Fluid Mechanics* (submitted)	May 1999
906	Aref, H., and D. L. Vainchtein	The equation of state of a foam—*Physics of Fluids* **12**, 23–28 (2000)	May 1999
907	Subramanian, S. J., and P. Sofronis	Modeling of the interaction between densification mechanisms in powder compaction—*International Journal of Solids and Structures*, in press (2000)	May 1999
908	Aref, H., and M. A. Stremler	Four-vortex motion with zero total circulation and impulse—*Physics of Fluids* **11**, 3704-3715	May 1999

List of Recent TAM Reports (cont'd)

No.	Authors	Title	Date
909	Adrian, R. J., K. T. Christensen, and Z.-C. Liu	On the analysis and interpretation of turbulent velocity fields—*Experiments in Fluids* **29**, 275–290 (2000)	May 1999
910	Fried, E., and S. Sellers	Theory for atomic diffusion on fixed and deformable crystal lattices—*Journal of Elasticity* **59**, 67–81 (2000)	June 1999
911	Sofronis, P., and N. Aravas	Hydrogen induced shear localization of the plastic flow in metals and alloys—*European Journal of Mechanics/A Solids* (submitted)	June 1999
912	Anderson, D. R., D. E. Carlson, and E. Fried	A continuum-mechanical theory for nematic elastomers—*Journal of Elasticity* **56**, 33–58 (1999)	June 1999
913	Riahi, D. N.	High Rayleigh number convection in a rotating melt during alloy solidification—*Recent Developments in Crystal Growth Research* **2**, 211–222 (2000)	July 1999
914	Riahi, D. N.	Buoyancy driven flow in a rotating low Prandtl number melt during alloy solidification—*Current Topics in Crystal Growth Research* **5**, 151–161 (2000)	July 1999
915	Adrian, R. J.	On the physical space equation for large-eddy simulation of inhomogeneous turbulence—*Physics of Fluids* (submitted)	July 1999
916	Riahi, D. N.	Wave and vortex generation and interaction in turbulent channel flow between wavy boundaries—*Journal of Mathematical Fluid Mechanics* (submitted)	July 1999
917	Boyland, P. L., M. A. Stremler, and H. Aref	Topological fluid mechanics of point vortex motions	July 1999
918	Riahi, D. N.	Effects of a vertical magnetic field on chimney convection in a mushy layer—*Journal of Crystal Growth* **216**, 501–511 (2000)	Aug. 1999
919	Riahi, D. N.	Boundary mode–vortex interaction in turbulent channel flow over a non-wavy rough wall—*Proceedings of the Royal Society of London A* (submitted)	Sept. 1999
920	Block, G. I., J. G. Harris, and T. Hayat	Measurement models for ultrasonic nondestructive evaluation—*IEEE Transactions on Ultrasonics, Ferroelectrics, and Frequency Control* **47**, 604–611 (2000)	Sept. 1999
921	Zhang, S., and K. J. Hsia	Modeling the fracture of a sandwich structure due to cavitation in a ductile adhesive layer—*Journal of Applied Mechanics* (submitted)	Sept. 1999
922	Nimmagadda, P. B. R., and P. Sofronis	Leading order asymptotics at sharp fiber corners in creeping-matrix composite materials	Oct. 1999
923	Yoo, S., and D. N. Riahi	Effects of a moving wavy boundary on channel flow instabilities—*Theoretical and Computational Fluid Dynamics* (submitted)	Nov. 1999
924	Adrian, R. J., C. D. Meinhart, and C. D. Tomkins	Vortex organization in the outer region of the turbulent boundary layer—*Journal of Fluid Mechanics* **422**, 1–53 (2000)	Nov. 1999
925	Riahi, D. N., and A. T. Hsui	Finite amplitude thermal convection with variable gravity—*International Journal of Mathematics and Mathematical Sciences* **25**, 153–165 (2001)	Dec. 1999
926	Kwok, W. Y., R. D. Moser, and J. Jiménez	A critical evaluation of the resolution properties of *B*-spline and compact finite difference methods—*Journal of Computational Physics* (submitted)	Feb. 2000
927	Ferry, J. P., and S. Balachandar	A fast Eulerian method for two-phase flow—*International Journal of Multiphase Flow*, in press (2000)	Feb. 2000
928	Thoroddsen, S. T., and K. Takehara	The coalescence–cascade of a drop—*Physics of Fluids* **12**, 1257–1265 (2000)	Feb. 2000
929	Liu, Z.-C., R. J. Adrian, and T. J. Hanratty	Large-scale modes of turbulent channel flow: Transport and structure—*Journal of Fluid Mechanics* (submitted)	Feb. 2000

List of Recent TAM Reports (cont'd)

No.	Authors	Title	Date
930	Borodai, S. G., and R. D. Moser	The numerical decomposition of turbulent fluctuations in a compressible boundary layer—*Theoretical and Computational Fluid Dynamics* (submitted)	Mar. 2000
931	Balachandar, S., and F. M. Najjar	Optimal two-dimensional models for wake flows—*Physics of Fluids*, in press (2000)	Mar. 2000
932	Yoon, H. S., K. V. Sharp, D. F. Hill, R. J. Adrian, S. Balachandar, M. Y. Ha, and K. Kar	Integrated experimental and computational approach to simulation of flow in a stirred tank—*Chemical Engineering Sciences* (submitted)	Mar. 2000
933	Sakakibara, J., Hishida, K., and W. R. C. Phillips	On the vortical structure in a plane impinging jet—*Journal of Fluid Mechanics* **434**, 273–300 (2001)	Apr. 2000
934	Phillips, W. R. C.	Eulerian space–time correlations in turbulent shear flows	Apr. 2000
935	Hsui, A. T., and D. N. Riahi	Onset of thermal–chemical convection with crystallization within a binary fluid and its geological implications—*Geochemistry, Geophysics, Geosystems*, in press (2001)	Apr. 2000
936	Cermelli, P., E. Fried, and S. Sellers	Configurational stress, yield, and flow in rate-independent plasticity—*Proceedings of the Royal Society of London A* **457**, 1447–1467 (2001)	Apr. 2000
937	Adrian, R. J., C. Meneveau, R. D. Moser, and J. J. Riley	Final report on 'Turbulence Measurements for Large-Eddy Simulation' workshop	Apr. 2000
938	Bagchi, P., and S. Balachandar	Linearly varying ambient flow past a sphere at finite Reynolds number—Part 1: Wake structure and forces in steady straining flow	Apr. 2000
939	Gioia, G., A. DeSimone, M. Ortiz, and A. M. Cuitiño	Folding energetics in thin-film diaphragms	Apr. 2000
940	Chaïeb, S., and G. H. McKinley	Mixing immiscible fluids: Drainage induced cusp formation	May 2000
941	Thoroddsen, S. T., and A. Q. Shen	Granular jets	May 2000
942	Riahi, D. N.	Non-axisymmetric chimney convection in a mushy layer under a high-gravity environment—In *Centrifugal Materials Processing* (L. L. Regel and W. R. Wilcox, eds.), in press (2000)	May 2000
943	Christensen, K. T., S. M. Soloff, and R. J. Adrian	PIV Sleuth: Integrated particle image velocimetry interrogation/validation software	May 2000
944	Wang, J., N. R. Sottos, and R. L. Weaver	Laser induced thin film spallation—*Experimental Mechanics* (submitted)	May 2000
945	Riahi, D. N.	Magnetohydrodynamic effects in high gravity convection during alloy solidification—In *Centrifugal Materials Processing* (L. L. Regel and W. R. Wilcox, eds.), in press (2000)	June 2000
946	Gioia, G., Y. Wang, and A. M. Cuitiño	The energetics of heterogeneous deformation in open-cell solid foams	June 2000
947	Kessler, M. R., and S. R. White	Self-activated healing of delamination damage in woven composites—*Composites A: Applied Science and Manufacturing* **32**, 683–699 (2001)	June 2000
948	Phillips, W. R. C.	On the pseudomomentum and generalized Stokes drift in a spectrum of rotational waves—*Journal of Fluid Mechanics* **430**, 209–229 (2001)	July 2000
949	Hsui, A. T., and D. N. Riahi	Does the Earth's nonuniform gravitational field affect its mantle convection?—*Physics of the Earth and Planetary Interiors* (submitted)	July 2000
950	Phillips, J. W.	Abstract Book, 20th International Congress of Theoretical and Applied Mechanics (27 August – 2 September, 2000, Chicago)	July 2000

List of Recent TAM Reports (cont'd)

No.	Authors	Title	Date
951	Vainchtein, D. L., and H. Aref	Morphological transition in compressible foam—*Physics of Fluids* (submitted)	July 2000
952	Chaïeb, S., E. Sato-Matsuo, and T. Tanaka	Shrinking-induced instabilities in gels	July 2000
953	Riahi, D. N., and A. T. Hsui	A theoretical investigation of high Rayleigh number convection in a nonuniform gravitational field—*Acta Mechanica* (submitted)	Aug. 2000
954	Riahi, D. N.	Effects of centrifugal and Coriolis forces on a hydromagnetic chimney convection in a mushy layer—*Journal of Crystal Growth*, in press (2001)	Aug. 2000
955	Fried, E.	An elementary molecular-statistical basis for the Mooney and Rivlin–Saunders theories of rubber-elasticity—*Journal of the Mechanics and Physics of Solids*, in press (2001)	Sept. 2000
956	Phillips, W. R. C.	On an instability to Langmuir circulations and the role of Prandtl and Richardson numbers—*Journal of Fluid Mechanics*, in press (2001)	Sept. 2000
957	Chaïeb, S., and J. Sutin	Growth of myelin figures made of water soluble surfactant—Proceedings of the 1st Annual International IEEE–EMBS Conference on Microtechnologies in Medicine and Biology (October 2000, Lyon, France), 345–348	Oct. 2000
958	Christensen, K. T., and R. J. Adrian	Statistical evidence of hairpin vortex packets in wall turbulence—*Journal of Fluid Mechanics* **431**, 433–443 (2001)	Oct. 2000
959	Kuznetsov, I. R., and D. S. Stewart	Modeling the thermal expansion boundary layer during the combustion of energetic materials—*Combustion and Flame*, in press (2001)	Oct. 2000
960	Zhang, S., K. J. Hsia, and A. J. Pearlstein	Potential flow model of cavitation-induced interfacial fracture in a confined ductile layer—*Journal of the Mechanics and Physics of Solids* (submitted)	Nov. 2000
961	Sharp, K. V., R. J. Adrian, J. G. Santiago, and J. I. Molho	Liquid flows in microchannels—Chapter 6 of *CRC Handbook of MEMS* (M. Gad-el-Hak, ed.) (2001)	Nov. 2000
962	Harris, J. G.	Rayleigh wave propagation in curved waveguides—*Wave Motion*, in press (2001)	Jan. 2001
963	Dong, F., A. T. Hsui, and D. N. Riahi	A stability analysis and some numerical computations for thermal convection with a variable buoyancy factor—*Geophysical and Astrophysical Fluid Dynamics* (submitted)	Jan. 2001
964	Phillips, W. R. C.	Langmuir circulations beneath growing or decaying surface waves—*Journal of Fluid Mechanics* (submitted)	Jan. 2001
965	Bdzil, J. B., D. S. Stewart, and T. L. Jackson	Program burn algorithms based on detonation shock dynamics—*Journal of Computational Physics* (submitted)	Jan. 2001
966	Bagchi, P., and S. Balachandar	Linearly varying ambient flow past a sphere at finite Reynolds number: Part 2—Equation of motion—*Journal of Fluid Mechanics* (submitted)	Feb. 2001
967	Cermelli, P., and E. Fried	The evolution equation for a disclination in a nematic fluid—*Proceedings of the Royal Society A* (submitted)	Apr. 2001
968	Riahi, D. N.	Effects of rotation on convection in a porous layer during alloy solidification—Chapter in *Transport Phenomena in Porous Media* (D. B. Ingham and I. Pop, eds.), Oxford: Elsevier Science (2001)	Apr. 2001
969	Damljanovic, V., and R. L. Weaver	Elastic waves in cylindrical waveguides of arbitrary cross section—*Journal of Sound and Vibration* (submitted)	May 2001
970	Gioia, G., and A. M. Cuitiño	Two-phase densification of cohesive granular aggregates	May 2001
971	Subramanian, S. J., and P. Sofronis	Calculation of a constitutive potential for isostatic powder compaction—*International Journal of Mechanical Sciences* (submitted)	June 2001